water

MDPI

*Article*

# Morphometric-Based Flash Flood Susceptibility and Hydrological Hazard Modeling: Implications for Sustainable Development in the Southern Red Sea Coast of Saudi Arabia

**Maan Okayli, Abdullah M. Alanazi and Bashar Bashir ***

Department of Civil Engineering, College of Engineering, King Saud University, P.O. Box 800, Riyadh 11421, Saudi Arabia; mokayli@ksu.edu.sa (M.O.); amalenazi@ksu.edu.sa (A.M.A.)
* Correspondence: bbashir@ksu.edu.sa

**Abstract**

Flash flood events are among the most critical hydrological hazards in arid and semi-arid regions, posing extreme threats to critical infrastructure, human safety, and sustainable development plans. This paper evaluates the flash flood susceptibility of the Al'Ataya catchment, a key watershed on the southern Red Sea coast, using an integrated geospatial analysis approach. To assess and quantify the flood hazard, we investigated 15 morphometric parameters for 24 particular sub-catchments within a sixth-order drainage system. Two complementary methods, the Morphometric Ranking Method and El-Shamy's approach, were utilized to classify the catchment into different flood susceptibility levels. Results from the Ranking Method identified seven sub-catchments (SC-2, SC-3, SC-6, SC-7, SC-8, SC-9, and SC-19) as having high flood hazard levels, mainly driven by large watershed areas, steep slopes, and high relief ratios. In contrast, El-Shamy's approach resulted in a different evaluation, identifying sub-catchments in Zone B (SC-23, SC-16, SC-17, SC-15, SC-6, SC-20) as high hazard sub-catchments due to the particular relationship between the bifurcation ratio parameter and the drainage density and stream frequency parameters. The integration of the two methods suggests that the susceptibility factor is controlled by the combined influence of a low drainage density and steep mountainous terrain draining toward the coastal zone. These results provide a spatial model for flood mitigation and early warning systems, supporting Saudi Vision 2030 through improvement to the development of southern urban centers such as Al'Ataya and Sabya.

**Keywords:** flash flood assessment; geospatial analysis; southern Red Sea coast; Saudi Vision 2030

Check for updates

Academic Editor: Masrur Ahmed

Received: 19 May 2026
Revised: 26 June 2026
Accepted: 28 June 2026
Published: 2 July 2026

**Copyright:** © 2026 by the authors. Licensee MDPI, Basel, Switzerland. This article is an open access article distributed under the terms and conditions of the Creative Commons Attribution (CC BY) license.

## 1. Introduction

Worldwide, natural hazards are phenomena that pose risks to particular areas and times [1]. Among these natural hazards, severe flash flood events represent some of the most unpredictable and destructive natural hazards due to their rapid onset and short duration, frequently overwhelming existing emergency response plans and disrupting critical infrastructure [2–4]. Floods are hydrometeorological hazards generated by extreme rainfall over relatively small areas, resulting in rapid increases in surface runoff and sudden peak discharges in drainage systems [5,6]. Due to climate change, the flash flood hazard is expected to increase in arid to semi-arid areas due to the increasing frequency and intensity of extreme rainfall events and reduced surface permeability [7,8].

The magnitude of flash floods is mainly controlled by the duration and intensity of precipitation; however, other geomorphological aspects, including drainage network characteristics and soil infiltration, also play an important role in controlling flash flood behavior and impacts [9–11]. Various catchments, as primary geomorphic units within hydrologic systems, provide a useful framework for understanding and managing extreme hydrological events [10,12]. Geospatial techniques provide effective methods for investigating arid and semi-arid regions like those in Saudi Arabia, where flash flood events are frequently triggered by heavy rainfall events and characterized by steep slopes and rugged topography [8,13]. Flood hazard assessment has become highly important for protecting infrastructure and communities and supporting sustainable regional development [14–16]. Therefore, in recent years, numerous significant studies have been performed to evaluate flood hazards in different critical regions [12,17–20]. Ref. [17] applied a morphometric analysis using geospatial methods to study the geometric characteristics of the Wadi Assuit catchment in Egypt and delineate the flood hazard potential zones. The socioeconomic impacts of floods in Pakistan, studied using geospatial analysis and literature synthesis, were discussed by the authors in Ref. [21]. Their paper emphasized the severity of flood hazards and focused on the importance of developing flood mitigation and management plans. In Italy, Ref. [22] applied topographical factors for assessing the similarity in flood-triggering factors, produced flood susceptibility maps, and evaluated the accuracy of the resulting flood susceptibility maps. In Bangladesh, Ref. [23] investigated the relationship of several morphometric factors with flood susceptibility and improved the flood susceptibility map of the Karnaphuli and Sangu River catchments in Bangladesh. In Turkey, Ref. [12] utilized a Morphometric Ranking Method using remote sensing techniques and geographic information systems (GIS) to evaluate flood susceptibility in the Mediterranean region of Turkey. Saudi Arabia has also given full attention to flood hazards because of the presence of strategically important regions targeted for sustainable development [24–28]. Ref. [24] evaluated flood hazards for urban areas in Riyadh, Saudi Arabia. Since the Riyadh watershed lacked observed rainfall and discharge, and had rainfall data of various return frequencies, the authors discussed the impact of watershed characteristics by running simulations at different urbanization levels. The flood hazard in the Wadi Al-Lith basin in Saudi Arabia was mapped and assessed in Ref. [28]. They used GIS and the AHP method to help control authorities and decision-makers in understanding flood hazard analysis, defining suitable mitigation models, and enabling nearby communities to develop preparedness plans for future flood events. Ref. [29] identified zones that are highly vulnerable to the flood hazard in Najran City in Southern Saudi Arabia using digital elevation model (DEM) data and GIS techniques. The Wadi Hali basin in the southwestern part of Saudi Arabia was examined in Ref. [20]. They developed a remote sensing model to locate high flood hazard zones and support flood hazard management by understanding the destructive impacts of flood events in the study basin.

Saudi Arabia is working hard to diversify its economy, develop major infrastructural projects along the Red Sea coastal zone, and support expanding urban communities in Jazan Province, and the flood hazard poses a critical risk to these development projects [13]. Currently, the application of modern tools and advanced techniques, including geospatial analysis, is essential for understanding flood hazards, as they permit a quantitative analysis of catchment characteristics in data-poor regions where ground hydrometric information is often insufficient [30–32]. Morphometric analysis, which includes the quantitative assessment of the physical aspects of a catchment, has been shown to be key for examining and understanding different hydrological processes [33–35]. By testing key morphometric parameters, such as the total catchment area, catchment perimeter, stream length, stream order, drainage density, stream frequency, and relief ratio, researchers can

understand how different catchments will respond to rainfall events and how susceptible they are to flooding [34–36]. Morphometric studies were first introduced in the pioneering Refs. [37,38], which developed methods to quantify and classify catchment and drainage network characteristics. Flood behaviors are highly influenced by the geomorphological features and drainage system characteristics of a catchment [9]. Variations in geomorphological and drainage characteristics can help in understanding significant differences in flood susceptibility between catchments and sub-catchments. This suggests that the accurate and detailed morphometric analysis of catchments and sub-catchments is essential for identifying the areas most susceptible to flooding [39–41].

Conventional flood susceptibility mapping is often based on single-index models, which introduce systematic bias due to parameter scaling effects. The applied Morphometric Ranking Method is a cumulative, scale-dependent method that combines absolute morphometric characteristics, including the total catchment area, catchment perimeter, and total stream length [9]. Because it effectively identifies large sub-catchments with large absolute runoff, this method is inherently biased toward larger catchments [5]. It commonly neglects smaller sub-catchments with steep relief that provide severe localized hazards [9]. Therefore, to adjust this limitation, a scale-independent method like El-Shamy's approach is integrated with the Ranked Method [9]. El-Shamy's approach describes the hydrographic flow routing efficiency of the drainage network by investigating relationships among bifurcation ratios, drainage density, and stream frequency parameters [41,42]. This method differentiates between rapid peak discharge generation and enhanced infiltration and groundwater recharge (high flood hazards and recharge, respectively) [42]. Additionally, because the El-Shamy approach acts as a scale-independent index, it may underestimate large catchments that produce large cumulative runoff volumes [43]. The critical rationale for integrating the ranked and El-Shamy approaches is to utilize their complementarity relationship [9,43]. This combination avoids the underestimation of catchments with efficient flow routing and a small total area, while preserving the representation of the catchment size and morphology-generating catchments with high runoff volumes [41,42].

To discuss these critical challenges, this study provides a high-resolution morphometric modeling for the Al'Ataya catchment using an integrated GIS-based dual-method approach. The novelty of this analysis lies in its dual approach, coupling the scale-dependent Morphometric Ranking Method with the scale-independent El-Shamy approach to distinguish between surface runoff potential and drainage network flow-routing efficiency. This study investigates three core research critical questions: (a) How do the morphometric properties of the studied 24 sub-catchments influence their spatial susceptibility to flooding events? (b) What tectonic and lithological controls clarify the differences in hazard assessment between cumulative ranking indices and drainage system efficiency curves? (c) How can these dual morphometric methods be used to evaluate observations from recent extreme flood events to support coastal development strategies? By addressing and discussing these significant issues, this study provides a high-resolution, spatial model that fills the gap between surface runoff production and coastal zone planning within the context of the climate change framework of the southern Saudi Red Sea coast.

## 2. Study Catchment

The southern Red Sea coastal zone of Saudi Arabia, particularly Jazan Province and its associated catchments, including the Al'Ataya catchment, present a natural laboratory for investigating flood hazards. This province is characterized by a significant geomorphological setting, including steep gradients, arid to semi-arid climatic conditions, and rapid socioeconomic expansion to achieve the goals of Saudi Arabia Vision 2030. This coastal zone is particularly vulnerable to floods because its climatic and geomorphological condi-

tions favor rapid surface runoff generation. The steep gradient between the As-Sarawat Mountains and the adjacent Tihama coastal plain zone generates a high-energy hydrological environment that accelerates water flow and enhances flash flood potential [20]. In these steep terrains, heavy rainfall often exceeds infiltration capacity, producing rapid runoff that is efficiently drained through various wadies, thereby increasing flood potential [44,45].

The Al'Ataya catchment, located in the Jazan Province in southwestern Saudi Arabia, is a geomorphologically significant watershed with considerable socioeconomic importance and sensitive environmental conditions. It is bounded by the mountainous zone divides to the north and east and by the Red Sea to the west (Figure 1). Covering a total area of approximately 1890.36 km$^2$, the study catchment extends between 16°50′ and 17°50′ North, and 34°00′ and 42°20′ East. The Al'Ataya catchment comprises several agricultural lands, expanding urban zones, and important infrastructure projects that are highly exposed to severe hydrological hazards, especially flash floods.

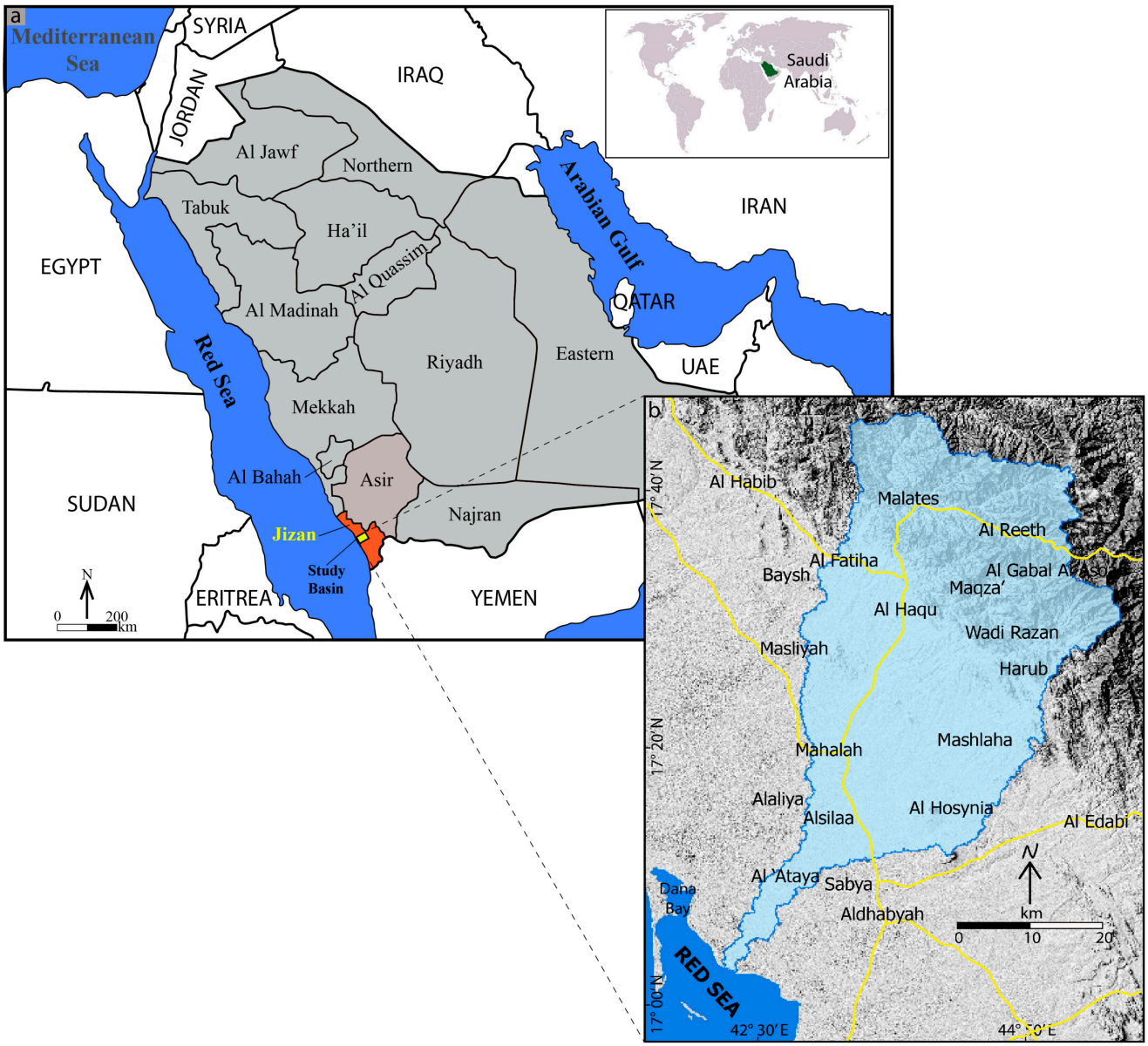



**Figure 1.** (**a**) Map of Saudi Arabian provinces, and (**b**) map of the Al'Ataya catchment.

The topography of Jizan Province is characterized by rugged relief and varied geomorphological features [46]. Elevations of the Al'Ataya catchment range from slightly below sea

level (−18 m as a minimum value) along the Red Sea coast to about 2461 m at the highest peaks in the eastern region of the catchment (Figure 2a). This critical elevation gradient is the main driver of the region's hydrological response, impacting runoff concentration, surface water flow velocity, and sediment transport rates [47]. The study catchment covers three different geomorphological units: (1) mountainous highlands near Al Habib and Al Reeth areas, characterized by steep slopes, ridges, and deeply incised channels such as Wadi Razan [47]. Moisture originating from the Red Sea is forced to raise over the mountainous headwaters, producing high-intensity rainfall events that generate flooding downstream; (2) a midstream transitional zone, including foothills and semi-sloped topography directing runoff from towns such as Maqza and Masliyah toward the coastal plain zone. Because of its the low elevation and low slopes, this zone, which includes settlements such as Al'Ataya, Baysh and Sabya, is highly vulnerable to flood inundation during flood events; and (3) the coastal plain of the Al'Ataya catchment area (Figure 2a). The slope profiles of the Al'Ataya catchment are important for modeling surface runoff velocity and its accumulation. Slope analysis of the Al'Ataya catchment suggests a broad range of gradients, between flat lands (0°) and 76.38° in the most rugged regions (Figure 2b). Slope gradients can be grouped into four basic zones reflecting the catchment hydrological features: (1) gentle (0–7.1°), which is located in the coastal plain near Dana Bay, (2) moderate (7.2–27.25), located in the transitional foothills zone between the mountainous zone and the coastal plain, (3) steep slopes (27.26–38.34°) observed in the mid-to-highland zones, and (4) very steep slopes (38.35–76.38°), located in the mountainous terrains near Al Habib and Al Reeth (Figure 2b).

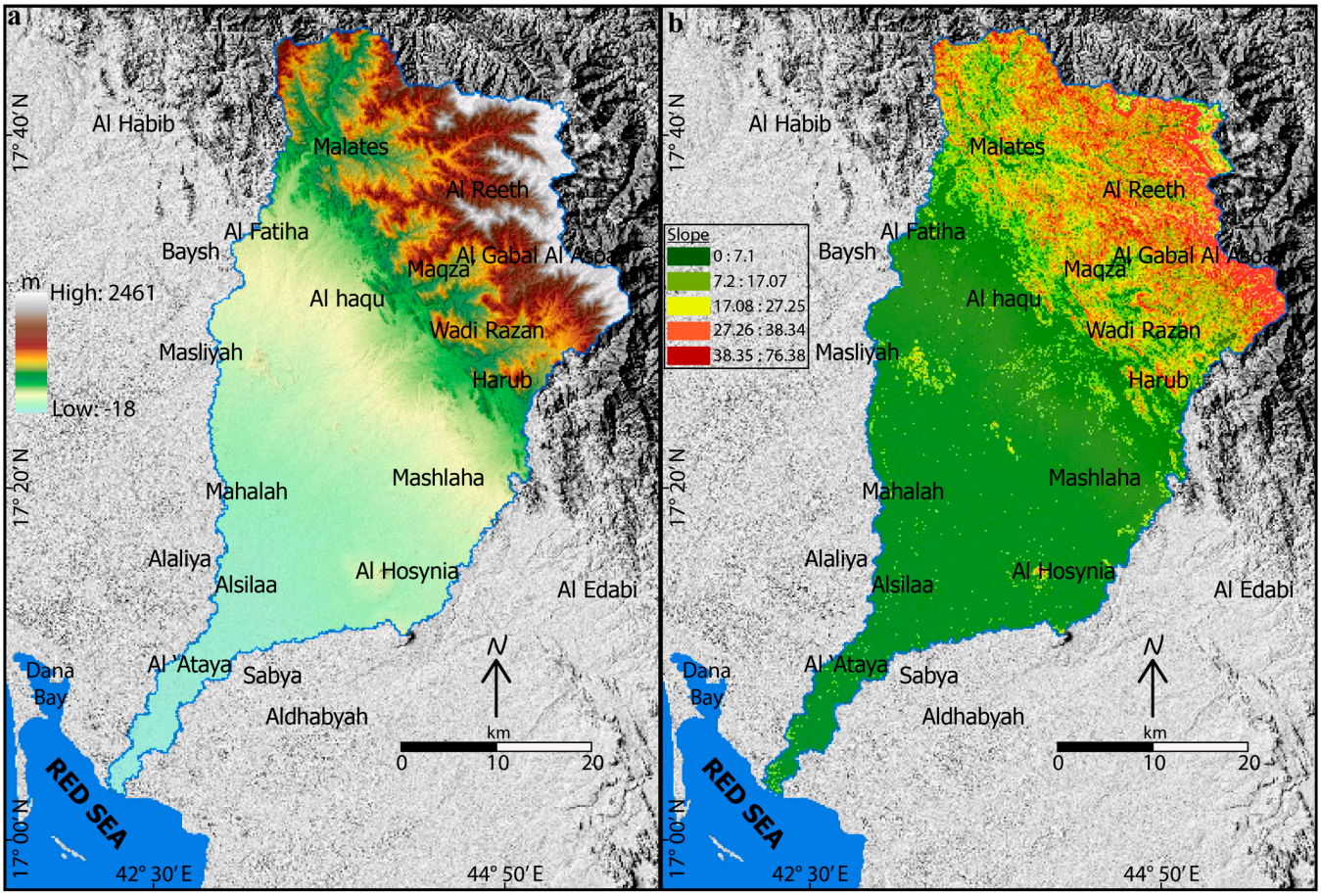



**Figure 2.** (**a**) Digital elevation model showing the general elevations, and (**b**) slope map of the Al'Ataya catchment.

The climatic conditions of the Al'Ataya catchment are described as arid to semi-arid, with a hot desert climate [48,49]. This region exhibits considerable seasonal differences in temperature and evaporation rates, ranging between ~6 mm/day and more than 12 mm/day in January and July, respectively, which highly influences surface water availability [50]. Jazan Province receives some of the highest rainfall recorded in Saudi Arabia, occurring as short-time, high-intensity storm events. Mean annual rainfall ranges between 80 mm along the Red Sea coast and 150 mm in the mountainous zones [47].

## 3. Materials and Methods

In this study, to effectively assess the flood hazard in the Al'Ataya catchment, an integrated model based on geospatial analysis, digital elevation model (DEM) data, and the powerful capabilities of the Geographic Information System software (ArcGIS 10.4) is required [51–54]. This integrated model has been successfully applied in several arid to semi-arid regions to study the hydrological and geomorphological processes [55–59]. The morphometric analysis approach is designed based on various processing techniques applied to digital elevation models (DEMs). High-spatial-resolution datasets, including the 12.5 m ALOS PALSAR and 30 m SRTM DEMs, were evaluated to assess the accuracy of the hydromorphological characterizations and visualization [59–61]. In this paper, the 12.5 m ALOS PALSAR DEM dataset was chosen to process over the 30 m SRTM DEM due to its superior resolution, which is very important to capture the intricate, deeply incised relief of the mountainous terrain headwaters of the study catchment. To support this high-spatial-resolution dataset, we conducted a comparison against an accurate local topographic map (control points) distributed over various terrain zones in the study catchment. This validation process confirmed that the topographic derivatives—in particular, slope and drainage patterns—are representative of ground conditions, through evaluation of the root mean square error (RMSE) within acceptable thresholds for hydrological modeling. All geospatial datasets and analyses applied in the current study were combined within a unified coordinate system and geographic data. The adopted coordinate system in this study was the Universal Transverse Mercator (UTM (Zone 37 N), referenced to the World Geodetic System 1984 datum (WGS 84)) [61,62]. Consequently, to ensure consistency within the unified vertical data of all DEMs, for vertical elevations, we referred to the Earth Gravitational Model 2008 [61]. For the current study, the 12.5 m DEM data was selected and applied for morphometrical and hydrological analyses to preserve topographic continuity and minimize topographic anomalies [61]. The morphohydrological analysis was conducted using QGIS 3.16 and ArcGIS 10.4 software [34,62].

In this study, voids and depressions were recorded and filled using a filling algorithm [60,63]. The drainage network extraction process was performed using the D8 flow algorithm within the ArcHydro toolset in ArcGIS 10.4 software. The 150-cell threshold was selected using a calibration process that included composing the extracted network with a high-resolution dataset. This particular threshold was detected to be the ideal compromise that effectively captured ephemeral channels recorded in the field while avoiding the generation of non-existent and artificial channels, thus preserving the hydrological integrity of the sixth-order drainage network (Figure 3) [6,60,63]. The steps of this processing are illustrated in Figure 3. According to the Strahler model of stream characterization, the drainage system in the current study exhibits a hierarchical pattern reaching up to sixth-order streams at the main study catchment outlet close to the Red Sea coast (Figure 4a). In the current study, sub-catchments were delineated due to the sixth-order drainage network. The process followed the hierarchical pattern approach where pour points were plotted at each main junction of next-order streams. This resulted in 24 distinct sub-catchments, confirming that the smallest units observed were hydrologically significant for the flood hazard

susceptibility assessment model while providing a comparative evaluation over the entire catchment [12,64]. Accordingly, sub-catchment delineation was conducted from the principal coastal outlet (sixth-order stream) upstream, presenting 24 distinct sub-catchments (1–24) [38] (Figure 4b). The spatial distribution of the drainage system and its various orders (first- to sixth-order streams) provide a key framework for measuring and evaluating the areal, linear and relief morphometric characteristics.

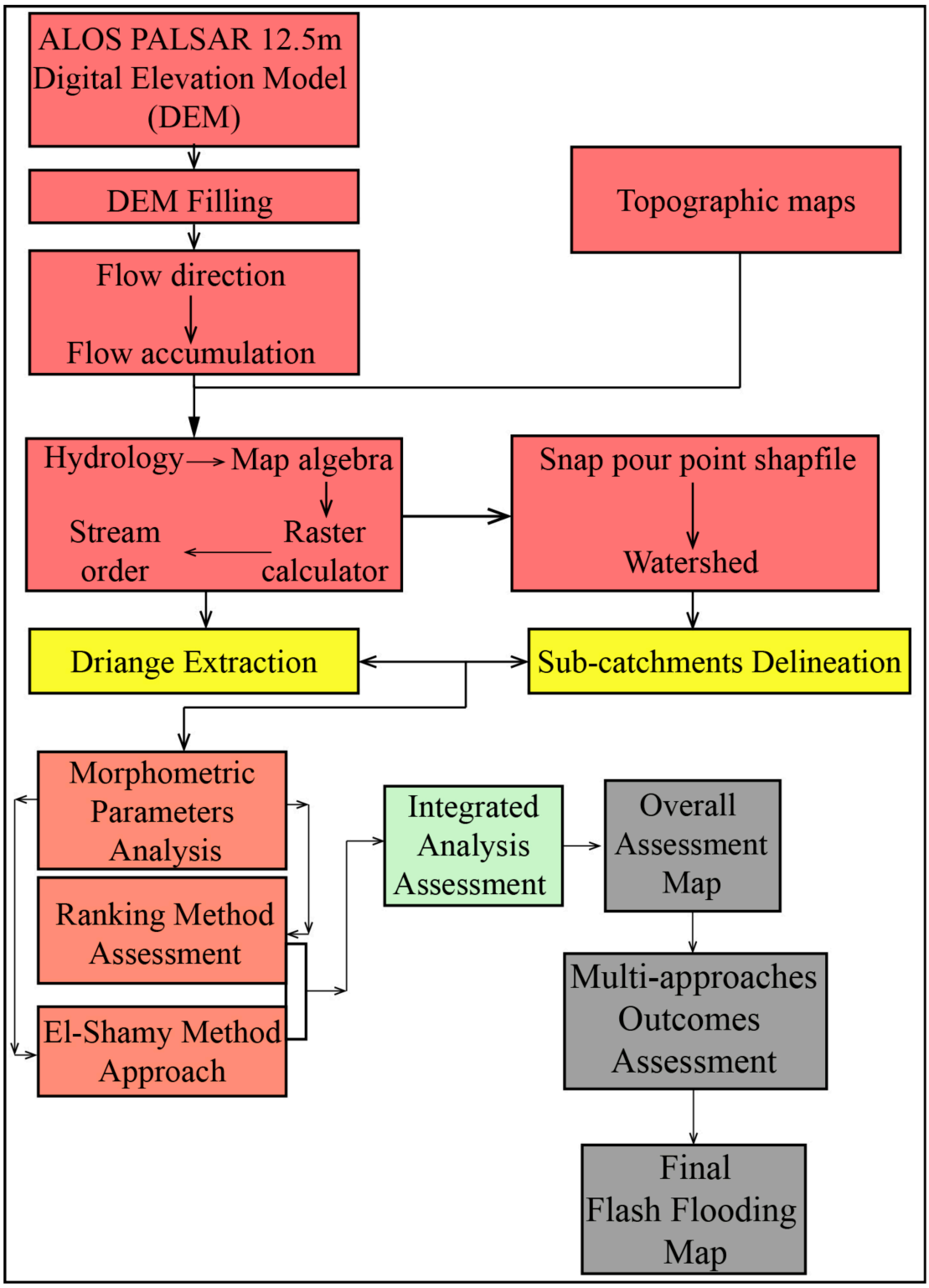



**Figure 3.** Flowchart showing the main processing step in the current study.

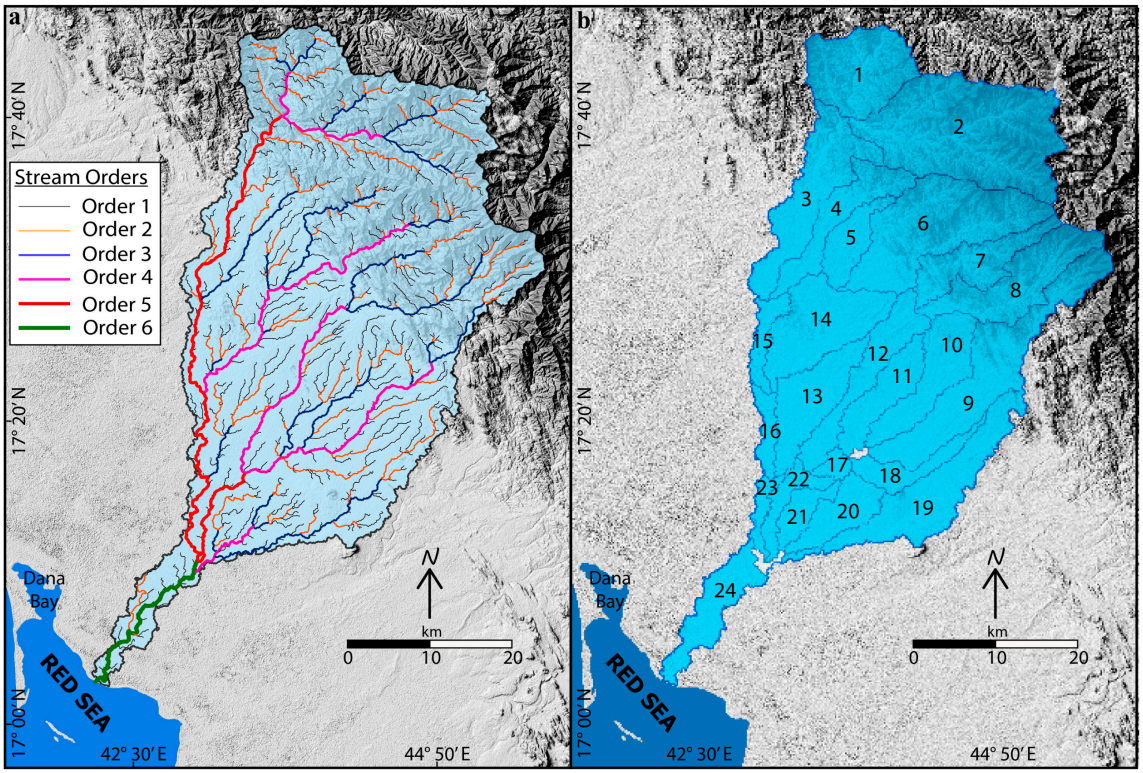



**Figure 4.** (**a**) Drainage network, and (**b**) sub-catchments of the Al'Ataya catchment.

### *3.1. Morphometric Parameters Analysis*

Effective morphometric parameters were calculated for each of the 24 delineated sub-catchments to assess their individual susceptibility to flash flood hazards. These morphometric parameters, including linear, areal, and relief characteristics, were estimated to present a comprehensive quantitative evaluation of the sub-catchments. Table 1 presents the morphometric parameters applied in the current study. Furthermore, these parameters were grouped into two distinct groups: (1) Group A including parameters that are positively correlated with flood hazard events (higher parameter values reflect higher rank of the flood hazard susceptibility), such as catchment area (A), stream frequency (Fs), and drainage density (Dd) [65,66], and (2) Group B includes parameters that exhibit an inverse relationship with flood hazard susceptibility, such as the elongation ratio (Re) [4,9].

**Table 1.** Morphometric parameters applied in the current study.

| Morphometric Parameters | Description and Formula | References |
|---|---|---|
| Total catchment area, A in km$^2$ | Total area of catchments | [37,67] |
| Catchment perimeter, P in km | Length of the outer boundary that encloses drainage catchments | [9,33] |
| Catchment length, L in km | Maximum length of a catchment that assigned parallel to the main catchment river | [33,38] |
| Stream order, Os | Hierarchical rank | [68,69] |
| Stream number, Ns | Ns = Ns1 + Ns2 + Ns3 + …. + Nsn | [33,70] |
| Total stream length, Ls in km | Ls = Ls1 + Ls2 + Ls3 +…. + Lsn | [71,72] |
| Stream frequency, Fs | Fs = Ns/A, where Ns is the total number of all-stream orders | [64,73] |
| Form factor, Ff | Ef = A/L$^2$ | [56,74] |
| Bifurcation ratio, Rb | Rb = Ns/Ns + 1, where Ns is the stream number value of any given order, and Nu + 1 is the stream number value for the following higher order | [75,76] |
| Drainage density, Dd | Dd = Ls/A | [34,77] |
| Texture ratio, Rt | Rt = Ns/P | [9,78] |
| Infiltration number, If | If = Fs/Dd | [56,79] |
| Elongation ratio, Re | Re = (2$\sqrt{}$A/$\pi$)/L | [35,76] |
| Catchment relief, R | R = H−h, where H and h are the highest and lowest elevation values of the given catchment, respectively | [6,9] |
| Ruggedness number, Nr | Nr = Dd × (R/1000) | [5,56] |
| Relief ratio, Rr | Rr = R/L | [64,75] |

### *3.2. Morphometric Ranking Method*

To assess flood susceptibility, the applied morphometric parameters were standardized through a linear normalization approach [80]. For Group A morphometric parameters (where values of the parameters are positively correlated with flood hazard susceptibility), the hazard rank was calculated using the following formula:

$$\text{Hazard Rank} = 2 \times \left( \frac{X - X_{\min}}{X_{\max} - X_{\min}} \right) + 1$$

For Group B morphometric parameters (where parameter values are conversely related to flood hazard susceptibility), the hazard rank is calculated using the following formula:

$$\text{Hazard Rank} = 2 \times \left( \frac{X - X_{\max}}{X_{\min} - X_{\max}} \right) + 1$$

where X represents the calculated value of the morphometric parameter for a given sub-catchment, and $X_{\max}$ and $X_{\min}$ represent the maximum and minimum values of that parameter among all 24 sub-catchments. After computing the ranking values of both Group A and Group B parameters, the average ranking result of each sub-catchment was calculated and applied to classify the studied sub-catchments into high, moderate, or low flood susceptibility classes [4,9,65].

### *3.3. Al-Shamy Approach*

In addition to the Morphometric Ranking Method, El-Shamy's approach assesses the relationship between three distinct morphometric parameters: drainage density (Dd), stream frequency (Fs), and bifurcation ratio (Rb) [9,41,42]. This method involves plotting stream frequency and drainage density parameters against the bifurcation ratio parameter on bivariate charts, categorizing the proposed 24 sub-catchments into three different hazard zones: high, moderate, and low. Zone C is characterized by high bifurcation ratio values in association with low stream frequency and drainage density values, reflecting suitable conditions for high groundwater recharge potential. Zone B suggests moderate conditions, providing a balance between flood hazard and water recharge potential. Zone A is defined by low values of the bifurcation ratio in association with high values of the stream frequency and drainage density, inferring high flood susceptibility and little groundwater recharge potential [9,80].

The dual methodology was performed as follows:

(1) Morphometric Ranking Method: Several parameters were analyzed using linear normalization. For a direct relation to hazard, we applied the equation $(X - X_{\min})/(X_{\max} - X_{\min})$. For an inverse relation to hazard, we applied $(X - X_{\max})/(X_{\min} - X_{\max})$. This model provides a direct summation of indices, presenting an equal relative hazard ranking model.

(2) El-Shamy Approach: In this method, we drew bivariate charts of the stream frequency and drainage density against the bifurcation ratio. The categorization zones (A, B, and C) were recognized due to the particular grouping of sub-catchments in these chart regions, which show the difference between surface runoff-dominated sub-catchments (high flood susceptibility ranks) and recharge-dominated sub-catchments (low flood susceptibility ranks).

The entire processing flowchart, including DEM pre-processing, sink-filling procedures, and the normalization equations, were effectively applied to confirm methodological consistency. As the parameter thresholds and justifications properties are explicitly detected, this methodology can be applied to other arid and semi-arid regions elsewhere, particularly to those whose flood hazard yield is poorly defined.

## 4. Results and Discussion

### *4.1. Morphometric Parameters' Characterization*

The applied quantitative morphometric analysis of the 24 sub-catchments confirms a high degree of heterogeneity of the study catchment. The sub-catchment areas range from 254.14 km$^2$ and 10.89 km$^2$ in Sub-c 2 and Sub-c 17, respectively (Table 2). Sub-catchments located in the upstream terrains indicate the highest elevations as 2461 m in sub-c 8 and 2217 m in sub-c 9, resulting in substantial relief, which enhances rapid runoff production. Sub-catchment lengths also vary considerably, ranging from 4.57 km and 111.61 km in sub-catchments 17 and 19, respectively, suggesting that longer and larger sub-catchments (sub-c 17 and sub-c 19) have the potential to accumulate large runoff volumes, but they present longer concentration times and delayed hydrological responses to rainfall [9,13,81,82].

**Table 2.** Geometry values of the study sub-catchments; Sub-Cs = sub-catchments.

| Sub-Cs. | Total Area (km$^2$) | Perimeter (Km) | C. Length (km) | H (m) | H (m) |
|---|---|---|---|---|---|
| **1** | 106.83 | 44.73 | 11.44 | 1131 | 262 |
| **2** | 254.14 | 81.97 | 23.39 | 2038 | 263 |
| **3** | 113.81 | 85.46 | 24.43 | 704 | 114 |
| **4** | 67.88 | 65.80 | 20.8 | 850 | 112 |
| **5** | 41.23 | 38.87 | 13.07 | 491 | 139 |
| **6** | 176.62 | 77.77 | 27.46 | 1970 | 96 |
| **7** | 67.79 | 61.81 | 20.25 | 2017 | 200 |
| **8** | 99.92 | 70.57 | 23.95 | 2459 | 201 |
| **9** | 156.97 | 105.26 | 37.21 | 2217 | 63 |
| **10** | 78.85 | 56.28 | 20.2 | 514 | 63 |
| **11** | 56.88 | 48.93 | 17.68 | 222 | 52 |
| **12** | 72.18 | 72.33 | 25.28 | 248 | 43 |
| **13** | 80.69 | 59.59 | 20.5 | 196 | 38 |
| **14** | 111.51 | 61.21 | 18.52 | 242 | 64 |
| **15** | 25.23 | 41.75 | 11.61 | 215 | 65 |
| **16** | 20.57 | 37.63 | 11.48 | 87 | 38 |
| **17** | 10.89 | 16.89 | 4.57 | 74 | 44 |
| **18** | 35.36 | 49.22 | 19.26 | 272 | 53 |
| **19** | 122.27 | 111.61 | 34.62 | 344 | 17 |
| **20** | 49.13 | 42.90 | 13.43 | 130 | 23 |
| **21** | 26.59 | 31.25 | 11.2 | 69 | 21 |
| **22** | 27.80 | 45.82 | 12.09 | 66 | 18 |
| **23** | 16.21 | 40.07 | 9.98 | 55 | 19 |
| **24** | 64.30 | 74.18 | 19.61 | 34 | −18 |

The extracted drainage framework provides a sixth-order stream system model at the main catchment outlet (Figure 4a). The highest stream number (Ns) values were observed in Sub-c 2 and Sub-c 6 as 96 and 79, respectively (Table 3), indicating dense channels that conduct rapid surface runoff and efficient surface water conveyance [83,84]. The total stream length (Ls) recorded in this study is correlated with the sub-catchment area. In the current study, sub-catchments 2 and 6 indicated the highest total stream length values of 194.17 km and 170.40 km, respectively (Table 3). These values suggest their significance in accumulating and transporting large runoff volumes during the heavy convective storm events that commonly hit the Jazan Province [47–49]. Relief parameters including Rr, Rn, and H are among the most effective keys in controlling flood energy and runoff velocity [2,6,85]. Sub-catchments 7 and 8 reflect the highest topographical ratios in the study catchment, with values of 89.73 and 94.28, respectively (Table 3). These high values of the relief parameters are associated with very steep slopes (38.35–76.38°), especially in the areas surrounding the Al Reeth and Al Habib regions (Figure 2).

**Table 3.** Values of the morphometric parameters extracted from the 24 sub-catchments tested in this study.

| Sub-Cs | Ns | Ls | Rb | Fs | Ff | Rt | Dd | If | Rn | Rr | Re |
|---|---|---|---|---|---|---|---|---|---|---|---|
| **1** | 43 | 90.33 | 0.33 | 0.40 | 0.82 | 0.96 | 0.85 | 0.48 | 0.73 | 75.96 | 1.02 |
| **2** | 96 | 194.17 | 0.24 | 0.38 | 0.46 | 1.17 | 0.76 | 0.49 | 1.36 | 75.89 | 0.77 |
| **3** | 37 | 149.52 | 0.18 | 0.33 | 0.19 | 0.43 | 1.31 | 0.25 | 0.78 | 24.15 | 0.49 |
| **4** | 27 | 55.10 | 0.22 | 0.40 | 0.16 | 0.41 | 0.81 | 0.49 | 0.60 | 35.48 | 0.45 |
| **5** | 17 | 42.76 | 0.29 | 0.41 | 0.24 | 0.44 | 1.04 | 0.40 | 0.36 | 26.93 | 0.55 |
| **6** | 79 | 170.40 | 0.27 | 0.45 | 0.23 | 1.02 | 0.96 | 0.46 | 1.81 | 68.24 | 0.55 |
| **7** | 24 | 55.20 | 0.23 | 0.35 | 0.17 | 0.39 | 0.81 | 0.43 | 1.48 | 89.73 | 0.46 |
| **8** | 41 | 83.25 | 0.18 | 0.41 | 0.17 | 0.58 | 0.83 | 0.49 | 1.88 | 94.28 | 0.47 |
| **9** | 54 | 152.16 | 0.30 | 0.34 | 0.11 | 0.51 | 0.97 | 0.35 | 2.09 | 57.89 | 0.38 |
| **10** | 23 | 82.57 | 0.25 | 0.29 | 0.19 | 0.41 | 1.05 | 0.28 | 0.47 | 22.33 | 0.50 |
| **11** | 20 | 53.44 | 0.26 | 0.35 | 0.18 | 0.41 | 0.94 | 0.37 | 0.16 | 9.62 | 0.48 |
| **12** | 21 | 69.26 | 0.31 | 0.29 | 0.11 | 0.29 | 0.96 | 0.30 | 0.20 | 8.11 | 0.38 |
| **13** | 24 | 73.62 | 0.24 | 0.30 | 0.19 | 0.40 | 0.91 | 0.33 | 0.14 | 7.71 | 0.49 |
| **14** | 39 | 127.11 | 0.34 | 0.35 | 0.33 | 0.64 | 1.14 | 0.31 | 0.20 | 9.61 | 0.64 |
| **15** | 8 | 80.09 | 0.58 | 0.32 | 0.19 | 0.19 | 3.17 | 0.10 | 0.48 | 12.92 | 0.49 |
| **16** | 8 | 84.10 | 0.58 | 0.39 | 0.16 | 0.21 | 4.09 | 0.10 | 0.20 | 4.27 | 0.45 |
| **17** | 3 | 35.04 | 0.50 | 0.28 | 0.52 | 0.18 | 3.22 | 0.09 | 0.10 | 6.56 | 0.81 |
| **18** | 11 | 65.03 | 0.56 | 0.31 | 0.10 | 0.22 | 1.84 | 0.17 | 0.40 | 11.37 | 0.35 |
| **19** | 47 | 110.10 | 0.16 | 0.38 | 0.10 | 0.42 | 0.90 | 0.43 | 0.29 | 9.45 | 0.36 |
| **20** | 24 | 61.37 | 0.52 | 0.49 | 0.27 | 0.56 | 1.25 | 0.39 | 0.13 | 7.97 | 0.59 |
| **21** | 11 | 28.75 | 0.38 | 0.41 | 0.21 | 0.35 | 1.08 | 0.38 | 0.05 | 4.29 | 0.52 |
| **22** | 8 | 24.36 | 0.14 | 0.29 | 0.19 | 0.17 | 0.88 | 0.33 | 0.04 | 3.97 | 0.49 |
| **23** | 4 | 77.52 | 0.33 | 0.25 | 0.16 | 0.10 | 4.78 | 0.05 | 0.17 | 3.61 | 0.46 |
| **24** | 21 | 77.72 | 0.54 | 0.33 | 0.17 | 0.28 | 1.21 | 0.27 | 0.06 | 2.65 | 0.46 |

In the current study, the mountainous terrain including sub-catchments 2, 6, 8, and 9) is occupied mainly by the Precambrian units of the Baysh Group as a part of the southern Arabian Shield [49]. These Precambrian units are mainly composed of impermeable, highly consolidated metadacites, metabasalts, and greenstones (Table 4) [86]. Because these rock units have little porosity, they produce high runoff rates (Table 4) [86]. In the adjacent Wadi Baysh with similar lithology, infiltration tests were performed. The results indicate that the massive Precambrian rocks act as a relatively impermeable surface, with runoff rates exceeding 0.35 during extreme storms (Table 4) [49,85,86]. These significant-runoff rates are enhanced by the tectonic framework of the study region. The high values of bifurcation ratios recorded in these mountainous highlands infer significant structural control, where drainage patterns are oriented along NNW-SSE joints, faults, and shear zones, produced from the Red Sea rifting [49]. This tectonic framework encourages a rapid, parallel drainage density, minimizing the concentration time and increasing the generation of downstream peak discharges (Table 4) [86].

In the transitional zone, these basement rocks are overlain by the sedimentary beds of Cambrian–Ordovician sandstone (Table 4). This sedimentary sequence is highly weathered and fractured (up to 20 m) [49]. Across this zone, infiltration investigation presents permeabilities ranging from 0.58 to 3.20 m/day, where the fractured rocks facilitate in observing moderate rates of the groundwater recharge [87]. Conversely, the coastal zone covering

sub-catchments 19 and 24 shows unconsolidated, thick, and deep alluvial deposits (10 to 100 m in depth) (Table 4) [49]. This succession comprises sand sheets and coarse gravel that exhibits high permeability and porosity [48]. Pumping tests performed on some water wells in the coastal zone show transmissivity values > $1.25 \times 10^{-2}$ $m^2/s$ and infiltration rates of ~37.15 m/day [49,88].

**Table 4.** Topographic, geological, structural, and hydrological characteristics of the major geomorphological domains in the study area.

| Topographical Domain | Geological Domain | Structural Features | Estimated Infiltration Rates | Investigated Hydrological Keys |
|---|---|---|---|---|
| Mountainous terrains (sub-catchments 2, 6, 8, and 9) | Crystalline basement rocks (Precambrian) | NNW-SSE-trending major lineaments (dense joint system) | Infiltration rate ≤0.15 m per day | High surface runoff rates (≥0.35) and high bifurcation ratio values (≥5) |
| Transition zone (sub-catchments 1, 4, and 10) | Sandstones (Cambrian–Ordovician) and carbonates (Jurassic) | Weathered zone in association normal faults | Permeability = (0.58–3.20 m per day) showing moderate recharge along assigned fractures | Moderate surface runoff rates and flow velocities |
| Coastal zone (sub-catchments 19 and 24) | Unconsolidated alluvial deposits, gravels, silt, and coarse sands (Quaternary) | Red sea coastal tectonic features (half grabens and structural rifting) | Permeability = (12.5–37.15 m per day) showing high transmissivity rate ($1.25 \times 10^{-2}$ $m^2/s$) | Groundwater recharge = 72.08 mm per year |

The annual recharge rate of the groundwater estimated for the coastal zone is observed as 72.08 mm/year, suggesting that the lower reaches of the study catchment have substantial groundwater-recharge potential [49]. Consequently, an abrupt decrease in flow velocity is observed in this plain zone because of the low-gradient terrain, despite the rapid inflow of surface runoff [50]. The lateral extension of floodwaters over these flat, highly permeable plains results in flooding, increasing the flood hazard susceptibility of these coastal zones, which act as regional floodwater storage and accumulation areas [50].

Additionally, the Red Sea coastal sub-catchments, including sub-catchment 24, show relief ratios as low as 2.65, reflecting gentle-relief slopes (0–7.1°) and low-relief terrain [3]. Although these zones do not generate rapid runoff, they are still highly vulnerable to flash flooding because they act as downstream storage areas for runoff arising from mountainous sub-catchments [83,89]. The low-lying area close to Dana Bay and Al'Ataya infers a significant reduction in water flow velocity, causing water to distribute laterally over vast areas of the Tihama coastal plain [30,90]. Therefore, these low-lying coastal plains are susceptible to flood inundation during significant runoff events.

The geographic framework of flood susceptibility in the Al'Ataya catchment is controlled by topographic relief, structural and geological characteristics, and flow dynamics [47,81]. Several upper sub-catchments, including sub-c 2, sub-c 6, sub-c 8, and sub-c9, are recognized by steep slopes (27.26–38.34°) and high-elevation terrain (2461 m) (Figure 2a,b) [91]. These zones are generally occupied by thin soils, which show limited infiltration capacity because of the predominance of impermeable and highly consolidated crystalline rocks of the Arabian Nubian Shield [92]. Accordingly, severe convective rainfall events produce rapid runoff, which is effectively traveled through highly incised valleys with high flow velocities and energy [93,94]. Conversely, the downstream coastal zone occupied by sub-c 24 is characterized by flat, gentle-relief, low slopes (0–7.1°) and thick, unconsolidated alluvial deposits that normally conduct high rates of infiltration. Although these low-lying zones are not the main surface runoff drivers, they serve as receivers of runoff sourcing from the mountainous regions and are therefore highly susceptible to extreme inundation during severe rainfall events [49,95]. As the steep slope wadis connect to the Tihama plain zone, the abrupt decline in surface gradient causes a rapid

drop in surface flow velocity [95]. This reduction process promotes the lateral expanding of a flood, producing extreme flooding and long-term inundation over the coastal zone [91].

### *4.2. Flash Flood Susceptibility Due to the Ranking Method*

The findings of the Morphometric Ranking Method classified the proposed 24 sub-catchments into three different hazard ranks based on the cumulative results of the 15 applied morphometric parameters (Table 5; Figure 5). The high flood hazard group (>2.0) covers seven sub-catchments: 2, 3, 6, 7, 8, 9, and 19. Sub-catchments 6, 9 and 2 recorded the highest aggregate hazard values as 2.58, 2.53 and 2.52, respectively. These sub-catchments are recognized by high stream numbers, large areas, and critically high relief ratios, making them the most flood-prone in the study catchment (Figure 5). The moderate flood hazard rank (1.5–2) covers the majority of the study catchment, with 16 sub-catchments, including sub-catchments 1, 4, 5, 10, 11, 12, 13, 14, 15, 16, 18, 20, 21, 22, 23, and 24. These sub-catchments suggest intermediate results between 1.53 and 2 for sub-catchments 22 and 4, presenting the lower and upper boundaries of this flood rank. The low flood hazard rank (<1.5) is recorded by a single sub-catchment (sub-c 17). This unique sub-catchment was classified as having a low flood hazard rank due to its minimal total area (10.89 km$^2$) and poorly developed drainage system (Ns = 3).

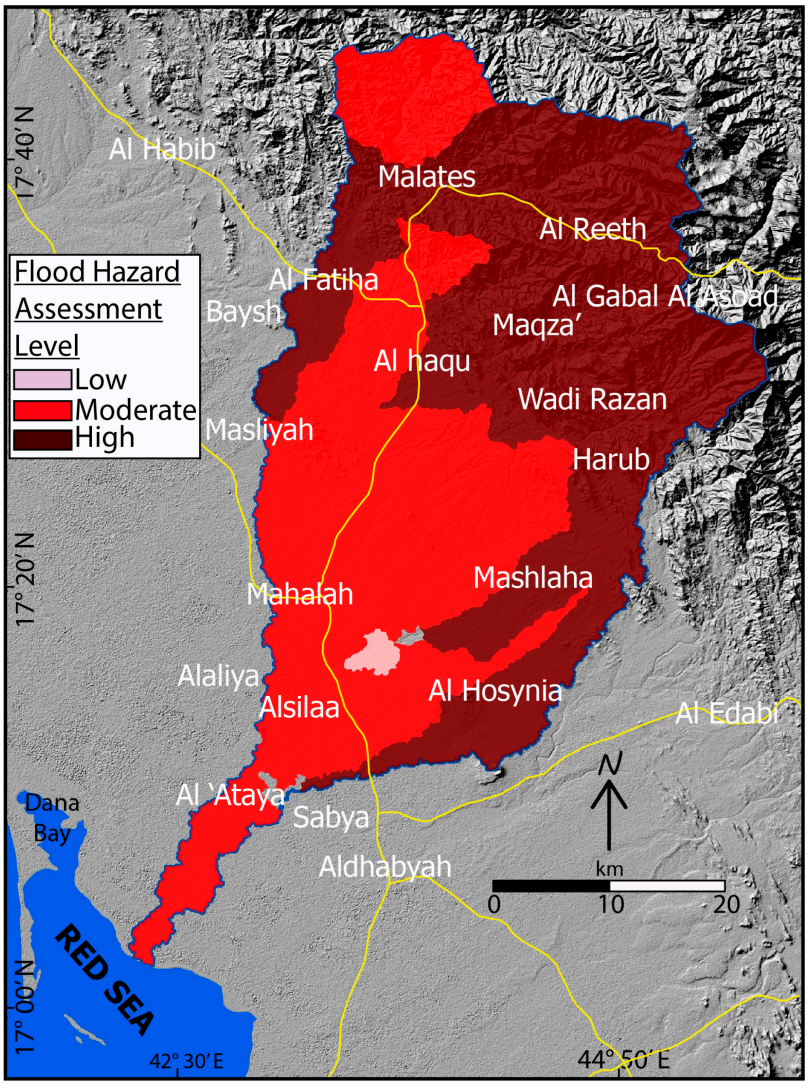



**Figure 5.** Flash flood susceptibility groups due to ranking hazard method.

**Table 5.** Ranking hazard method calculation for the proposed 24 sub-catchments.

| Sub-Cs | A | P | L | Ns | Ls | Rb | Fs | Ff | Rt | Dd | If | R | Rn | Rr | Re | Sum | Average | Hazard Rank |
|---|---|---|---|---|---|---|---|---|---|---|---|---|---|---|---|---|---|---|
| **1** | 1.79 | 1.59 | 1.42 | 1.86 | 1.78 | 1.86 | 2.29 | 1.00 | 2.61 | 1.04 | 2.92 | 1.75 | 1.68 | 2.60 | 1.00 | 27.18 | 1.94 | Moderate |
| **2** | 3.00 | 2.37 | 2.15 | 3.00 | 3.00 | 1.46 | 2.08 | 1.98 | 3.00 | 1.00 | 3.00 | 2.57 | 2.28 | 2.60 | 1.75 | 35.24 | 2.52 | High |
| **3** | 1.85 | 2.45 | 2.22 | 1.73 | 2.47 | 1.17 | 1.65 | 2.74 | 1.62 | 1.27 | 1.88 | 1.50 | 1.72 | 1.47 | 2.57 | 28.31 | 2.02 | High |
| **4** | 1.47 | 2.03 | 1.99 | 1.52 | 1.36 | 1.33 | 2.25 | 2.83 | 1.58 | 1.02 | 2.98 | 1.64 | 1.54 | 1.72 | 2.71 | 27.97 | 2.00 | Moderate |
| **5** | 1.25 | 1.46 | 1.52 | 1.30 | 1.22 | 1.68 | 2.37 | 2.59 | 1.63 | 1.14 | 2.56 | 1.29 | 1.32 | 1.53 | 2.39 | 25.24 | 1.80 | Moderate |
| **6** | 2.36 | 2.29 | 2.40 | 2.63 | 2.72 | 1.57 | 2.66 | 2.61 | 2.71 | 1.10 | 2.86 | 2.66 | 2.73 | 2.43 | 2.41 | 36.14 | 2.58 | High |
| **7** | 1.47 | 1.95 | 1.96 | 1.45 | 1.36 | 1.40 | 1.89 | 2.81 | 1.54 | 1.03 | 2.73 | 2.60 | 2.41 | 2.90 | 2.67 | 30.16 | 2.15 | High |
| **8** | 1.73 | 2.13 | 2.19 | 1.82 | 1.69 | 1.16 | 2.35 | 2.78 | 1.90 | 1.03 | 2.99 | 3.00 | 2.80 | 3.00 | 2.63 | 33.21 | 2.37 | High |
| **9** | 2.20 | 2.87 | 3.00 | 2.10 | 2.51 | 1.69 | 1.80 | 2.95 | 1.77 | 1.10 | 2.37 | 2.91 | 3.00 | 2.21 | 2.91 | 35.38 | 2.53 | High |
| **10** | 1.56 | 1.83 | 1.96 | 1.43 | 1.69 | 1.47 | 1.37 | 2.73 | 1.58 | 1.14 | 2.03 | 1.38 | 1.42 | 1.43 | 2.56 | 25.57 | 1.83 | Moderate |
| **11** | 1.38 | 1.68 | 1.80 | 1.37 | 1.34 | 1.52 | 1.87 | 2.76 | 1.58 | 1.09 | 2.46 | 1.13 | 1.11 | 1.15 | 2.60 | 24.84 | 1.77 | Moderate |
| **12** | 1.50 | 2.17 | 2.27 | 1.39 | 1.53 | 1.74 | 1.37 | 2.95 | 1.36 | 1.10 | 2.14 | 1.16 | 1.15 | 1.12 | 2.91 | 25.84 | 1.85 | Moderate |
| **13** | 1.57 | 1.90 | 1.98 | 1.45 | 1.58 | 1.45 | 1.42 | 2.73 | 1.57 | 1.07 | 2.24 | 1.11 | 1.10 | 1.11 | 2.56 | 24.85 | 1.78 | Moderate |
| **14** | 1.83 | 1.94 | 1.85 | 1.77 | 2.21 | 1.92 | 1.85 | 2.36 | 2.00 | 1.19 | 2.15 | 1.13 | 1.16 | 1.15 | 2.12 | 26.64 | 1.90 | Moderate |
| **15** | 1.12 | 1.52 | 1.43 | 1.11 | 1.66 | 3.00 | 1.58 | 2.75 | 1.17 | 2.20 | 1.22 | 1.11 | 1.42 | 1.22 | 2.58 | 25.09 | 1.79 | Moderate |
| **16** | 1.08 | 1.44 | 1.42 | 1.11 | 1.70 | 3.00 | 2.18 | 2.83 | 1.21 | 2.66 | 1.20 | 1.02 | 1.15 | 1.04 | 2.71 | 25.74 | 1.84 | Moderate |
| **17** | 1.00 | 1.00 | 1.00 | 1.00 | 1.13 | 2.62 | 1.24 | 1.82 | 1.15 | 2.22 | 1.15 | 1.00 | 1.05 | 1.09 | 1.61 | 20.07 | 1.43 | Low |
| **18** | 1.20 | 1.68 | 1.90 | 1.17 | 1.48 | 2.87 | 1.53 | 3.00 | 1.23 | 1.54 | 1.53 | 1.17 | 1.35 | 1.19 | 3.00 | 25.85 | 1.85 | Moderate |
| **19** | 1.92 | 3.00 | 2.84 | 1.95 | 2.01 | 1.07 | 2.14 | 2.98 | 1.60 | 1.07 | 2.69 | 1.27 | 1.25 | 1.15 | 2.96 | 29.89 | 2.14 | High |
| **20** | 1.31 | 1.55 | 1.54 | 1.45 | 1.44 | 2.73 | 3.00 | 2.51 | 1.86 | 1.24 | 2.53 | 1.07 | 1.09 | 1.12 | 2.28 | 26.72 | 1.91 | Moderate |
| **21** | 1.13 | 1.30 | 1.41 | 1.17 | 1.05 | 2.08 | 2.38 | 2.68 | 1.47 | 1.16 | 2.49 | 1.02 | 1.01 | 1.04 | 2.49 | 23.87 | 1.71 | Moderate |
| **22** | 1.14 | 1.61 | 1.46 | 1.11 | 1.00 | 1.00 | 1.34 | 2.74 | 1.14 | 1.06 | 2.25 | 1.02 | 1.00 | 1.03 | 2.57 | 21.46 | 1.53 | Moderate |
| **23** | 1.04 | 1.49 | 1.33 | 1.02 | 1.63 | 1.86 | 1.00 | 2.81 | 1.00 | 3.00 | 1.00 | 1.01 | 1.13 | 1.02 | 2.68 | 23.02 | 1.64 | Moderate |
| **24** | 1.44 | 2.21 | 1.92 | 1.39 | 1.63 | 2.80 | 1.66 | 2.80 | 1.34 | 1.22 | 1.99 | 1.02 | 1.02 | 1.00 | 2.66 | 26.10 | 1.86 | Moderate |

### *4.3. El-Shamy's Approach*

El-Shamy's dual analysis approach suggests a refined model of drainage network properties and flood susceptibility (Figure 6). The integrated results from the two dual charts suggest that high flood hazard ranks (Zone B) are represented by sub-catchments 23, 16, 17, 15, 6, and 20. Among this group, sub-catchments 23 and 16 present the highest drainage density values, at 4.78 km/km$^2$ and 4.09 km/km$^2$, respectively. Zone C, described as having a moderate rank of flood hazard, covers the sub-catchments 3, 22, 13, and 5 (Figure 6). Conversely, Zone A is recognized as having the lowest flood hazard susceptibility rank, including sub-catchments 2 and 9, that reflect low hydrological responses across the entire study catchment (Figure 6). These assigned sub-catchments (sub-c-2 and sub-c-9) which were described as high hazard zones in the Morphometric Ranking Method (Figure 5), reveal a methodological conflict of the two applied methods. The discrepancy is an indicator for sub-catchments 17 and 23. While the Morphometric Ranking Method assigns sub-c 17 as a low flood hazard unit because of its small area and low morphometric characteristics, El-Shamy's approach significantly identifies it as a high flood hazard unit (Zone B) because of its high drainage density value (3.22 km/km$^2$) and low bifurcation ratio value (0.50), suggesting a highly efficient drainage network structure.

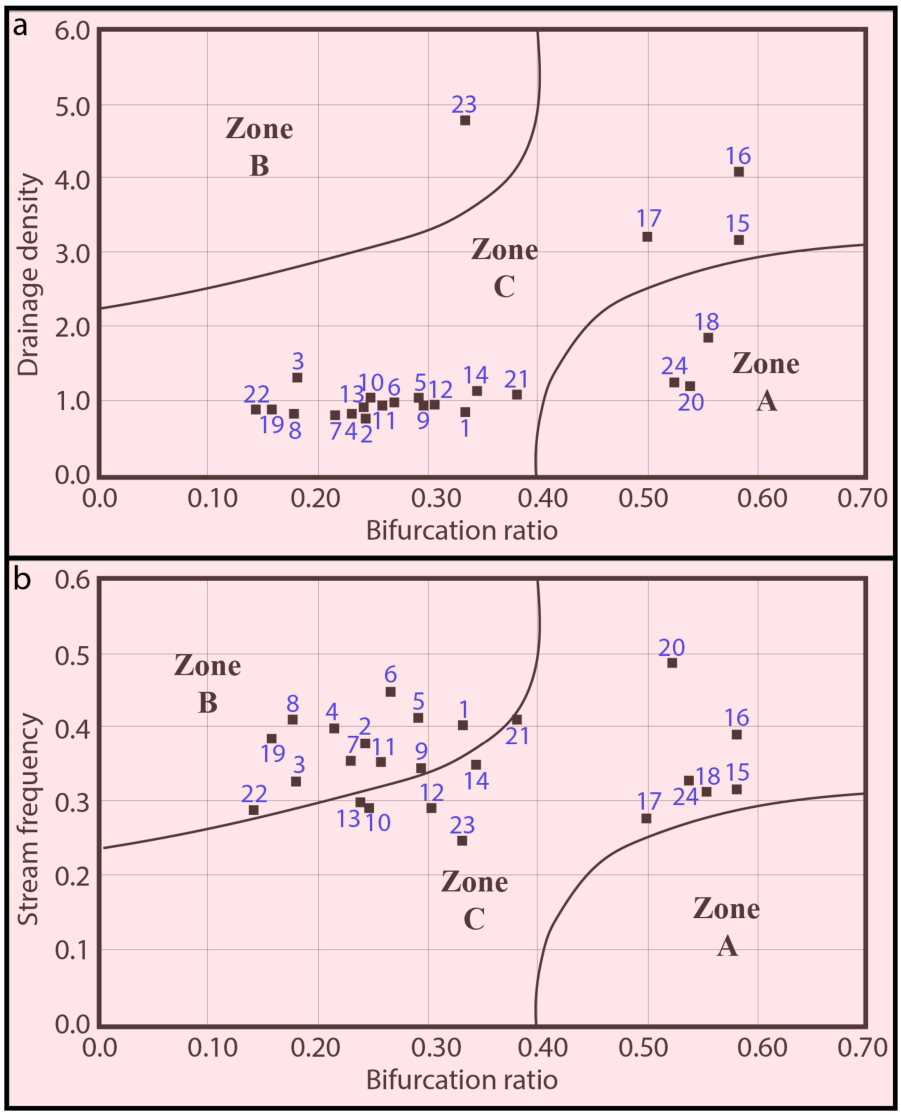



**Figure 6.** El-Shamy approach charts for evaluating flood susceptibility levels. (**a**) Rb against Dd, and (**b**) Rb against Fs.

The apparent inconsistency in flood hazard ranking for sub-catchments 17, 2, and 9 between the two applied models was derived from the fundamental differences between scale-dependent volumetric keys and scale-independent direct efficiency keys. The Morphometric Ranking Method is a measure-dependent index incorporating absolute catchment geometrical parameters, including the total area of the catchment (A), catchment perimeter (P), and total channel length (L) in its resulting model [81]. Sub-catchments 2 and 9 are among the largest sub-catchments in the study catchment, with total areas of Sub-c 2 = 254.14 $km^2$ and Sub-c 9 = 156.97 $km^2$, respectively (Table 3). Because larger catchments can accumulate absolute runoff volumes during intense events, they receive higher flood hazard ranks in the cumulative ranking framework. Conversely, El-Shamy's approach is a measure-independent index that assesses drainage system control on the surface runoff response [94]. It investigates the bifurcation ratio (Rb) values against drainage density (Dd) and stream frequency (Fs) values using two indicative charts. The physical and mathematical divergence in flood susceptibility categorization for sub-catchments 2, 9, and 17 is interpreted by the structural and geological differences in their sub-catchments. Sub-c 2 and sub-c 9 are mainly covered by the crystalline, impermeable greenstones of the basement Baysh Group. These large sub-catchments generate large cumulative runoff volumes. Although their elongated shapes result in a lower routing efficiency rank (Zone A) in El-Shamy's approach, they are correctly recognized as having a high flood hazard by the Morphometric Ranking Method due to their large total area. Conversely, sub-c 17 is a small catchment (10.89 $km^2$) that is assigned as having a low flood hazard by the Morphometric Ranking Method. Moreover, because it is characterized by high drainage density (3.22 $km/km^2$) and low bifurcation ratio (0.50) values, which are tectonically controlled by NNW-SSE-trending faults, El-Shamy's approach defines it as a high flood hazard zone (Zone B) [96]. The above discussion reveals that both methods used are more complementary than contradictory. The Morphometric Ranking Method records sub-catchments of high volumetric flood hazard potential, while El-Shamy's approach assigns significant hydrological responses and peak flow generation capacity [41,96].

### *4.4. Validation and Calibration of Empirical Models*

In 2024, The southern Red Sea coast experienced a critical climate-driven change in peak precipitation, resulting in a transition from the observed autumn rainfall peaks to severe summer events between October and August, respectively [97]. This extreme change was observed by a monthly rainfall total of 414.8 mm in August 2024 in comparison with the historical/recorded August rainfall average of 54.9 mm [97]. On 23 August, a daily precipitation event (113.7 mm) was observed, causing extreme flooding over the study region [97]. Moreover, on 1 August of the same year, a significant flood event occurred in the steep As-Sarawat terrains, causing the collapse of the main highway bridge on the important Jazan–Abha road [94]. In Table 5, the physical impacts and distributions of these historical/recorded events are gathered and compared to the flood susceptibility ranks for the studied sub-catchments.

The validation model indicates the high predictive capability of the dual-method approach. The high morphometric susceptibility assigned for sub-catchments 2, 6, and 9 corresponds to the source areas of high flow velocity that damaged the Jazan–Abha major bridge on 1 August 2024 [97]. The sub-catchments 2, 6, and 9 reveal high relief ratios (>75.89) and steep slopes (=38.35°:76.38°), triggering rapid surface runoff concentration (Table 6) [89]. The complementary idea of the El-Shamy approach is well correlated with sub-catchment 17. Sub-c 17 was identified as having a low rank of flood susceptibility by the Morphometric Ranking Method because of its small area (~10.89 $km^2$) (Table 2). Nevertheless, El-Shamy's approach assigned it as having a high

rank of flood susceptibility because of its low bifurcation ratio value (=0.50) and high drainage density value (=3.22 km/km$^2$), suggesting a highly effective drainage system efficiency [41]. Field records from the August 2024 event revealed that sub-c 17 produced high-velocity discharge volumes that ran through the main channel immediately after the storm event [97]. In contrast, large area sub-catchments, such as 2 and 9, which fall in El-Shamy's Zone A (Low rank) because of geometrical elongation, were correctly selected as having a high hazard rank by the second Ranking Method. This model is supported by the fact that their large spatial areas generate the large runoff volumes that characterize downstream flood events.

**Table 6.** Validation model of the flood susceptibility ranks.

| Sub-Catchments | Ranking Method Ranging | El-Shamy Approach Ranking | Historical Events and Location (August 2024) | Impacts |
|---|---|---|---|---|
| Sub-c 2 | High | Low | High velocity surface runoff (mountain terrain) | Channel incision and rock transportation |
| Sub-c 6 | High | High | Convergence of peak flow (upper Wadi Razan drainage system) | Rock stripping and local mountain roads' destruction |
| Sub-c 9 | High | Low | Severe mountainous runoff along Jazan–Abha transport road | Highway bridge collapsing on 1 August 2024 |
| Sub-c 17 | Low | High | Short-duration, local flow to the main wadi | Rapid flow, little sediment deposition, and small local ponding |
| Sub-c 19 | High | Moderate | Flood event (Sabya plain and regional coastal zone) | Widespread flood event and agricultural lands' inundation |
| Sub-c 24 | Moderate | Moderate | Coastal depositional zone (Dana Bay urban area) | Parts of coastal zone are submerged and water ponded for more than 72 h |

These validation findings are further confirmed by reservoir characteristics recorded at the same time. On 26 August 2024, the Saudi Arabia Irrigation Organization authority opened the Baysh Dam gates to discharge water and lower the level of the reservoir. At that particular time, the reservoir stored a significant volume of water, at 117.7 million m$^3$, which was getting close to its safe operating system limit of about 192.75 million m$^3$ [49,95]. This operational system was required to accommodate anticipated runoff water from future rainfall [49]. Additionally, it regulated and managed any sudden catastrophic event, as demonstrated by the failure of the Al-Lith Dam, which happened in November 2018 [48,98]. During that catastrophe, severe rainfall saturated the catchment and exceeded the capacity of the reservoir, producing a structural failure that let a large volume of water flow. The flood event inundated an area of ~100 km$^2$ downstream, immersing Al-Lith City, with water depths of about 30:100 cm [94]. This catastrophic event caused extreme damage to ~9505 residential properties and resulted in 75 fatalities [98]. The Al-Lith critical event reveals the high importance of geomorphometric flood risk models for supporting early warning systems and regulating reservoir levels during severe summer storm events in the critical Jazan Province.

### *4.5. Assumptions, Uncertainty and Limitations*

A comprehensive assessment of the flood susceptibility model requires the consideration of the inherent uncertainties, index assumptions, and overall limitations associated with the morphometric analysis:

(1) The proposed model suggests a uniform rainfall distribution over the total area of the Al'Ataya catchment. Moreover, Jizan Province experiences large orographic precipitations gradients, and high elevated terrains receive ~300 –600 mm/yr, while coastal zones receive ~ 80:120 mm/yr [48]. (2) The proposed model also suggests uniform infiltration rates over the entire catchment. Geology varies critically from eastern crystalline rocks of low-permeability conditions to highly permeable alluvium and gravels in the western wadi floors.

(3) Despite the ALOS DEM data providing an open-source high-resolution dataset, it is exposed to interpolation and relief-related errors in highly rugged valleys. These limitations can explain small inconsistencies in extracted morphometric parameters, including slope, relief, and ruggedness parameters.

### *4.6. Implications for Saudi 2030 Vision Sustainability Goals*

The integrated flood hazard assessment model provides a valuable framework for sustainable development planning in the coastal zone of the Jazan province. Modern studies suggest that rainfall intensity is the most critical source of flood hazard events in this region, followed by drainage density and morphometric characteristics of a given catchment. Several regions in the Arabian Peninsula received more than 250 mm within 24 h during severe flood events recorded in April 2024. This event reveals the rising severity of hydroclimatic hazards affecting significant infrastructure in Saudi Arabia [26]. Among the framework of Saudi Arabia Vision 2030, these results suggest that bridges, highways and projects close to Sabya and Al'Ataya must account for the high surface runoff generation potential of sub-catchments 2, 6, and 9. Additionally, sub-catchments marked by high infiltration rates could account for flood harvesting projects. Moreover, recent research studies in Wadi Baysh recorded infiltration rates of ~37.15 m/day, suggesting that flood events can be changed from a hydrogeohazard to a valuable main water resource [48]. Additionally, the Al'Ataya (Baysh) Dam experiences a high amount of sediment accumulation, which minimizes its flood capacity over a long duration [26]. Therefore, integrating real-time predictive hydrological and geospatial analysis into high flood hazard sub-catchments, such as sub-catchment 6, is essential for reservoir management.

## 5. Conclusions

This study reveals that flood hazard susceptibility over the southern Red Sea coast zone of Saudi Arabia is highly affected by a severe orographic rainfall gradient. Despite the coastal zone being characterized by arid to semi-arid climatic characteristics and receiving low annual rainfall (80–120 mm/yr), it remains highly susceptible to flood events produced in the humid highland terrains, where average annual precipitation generally ranges between 150 mm/yr and 300 mm/yr, and may exceed 600 mm during severe summer storms. Additionally, among the framework of Saudi Arabia's Vision 2030, which has triggered significant industrial, urban, and mega-infrastructure development in highly growing regions, including Sabya, the city of Jazan, and the Al'Ataya coastal region, flood hazard management plans should improve from reactive emergency plans to adaptive and proactive mitigation strategies. Flood conversion channels and their hydraulic characteristics should be modeled to regulate the main runoff volumes produced by the main upper sub-catchments, especially sub-catchments 2, 6, and 9, to minimize the flood hazard impact on downstream urban valleys. Moreover, effective warning systems are very important for regulating the fast hydrological response of highly responsive drainage systems, including those occupied by sub-catchments 17 and 23. Moreover, regional hazard plans should consider recent climatic changes, marked by increasing rainfall intensities and more severe convective events. The rising frequency of high-intensity rainfall storms across consecutive

periods may exceed the storage ability of the current reservoirs and overwhelm existing drainage systems. Accordingly, future flood protection plans must integrate real-time hydromorphometrical data, various meteorological monitoring and remote sensing observation stations, and dynamic flood-predicting systems. Such observations would help in filling the gap between static hazard evaluations and early warning systems. Integrating advanced morphometric analysis with high-accuracy monitoring and forecasting frameworks represents an important contribution toward enhancing flood hazard assessment and solving the problem of data-poor coastal zones.

**Author Contributions:** Conceptualization, B.B. and A.M.A.; methodology, B.B.; software, M.O.; validation, M.O., B.B. and A.M.A.; formal analysis, M.O.; investigation, A.M.A.; resources, B.B.; data curation, A.M.A.; writing—original draft preparation, B.B.; writing—review and editing, B.B.; visualization, M.O.; supervision, A.M.A.; project administration, B.B.; funding acquisition, B.B. All authors have read and agreed to the published version of the manuscript.

**Funding:** This research was supported by Ongoing Research Funding program (grant number ORF-2026-296), King Saud University, Riyadh, Saudi Arabia.

**Data Availability Statement:** The original contributions presented in this study are included in the article. Further inquiries can be directed to the corresponding author.

**Conflicts of Interest:** The authors declare no conflicts of interest.

## References

1. Alcántara-Ayala, I. Geomorphology, Natural Hazards, Vulnerability and Prevention of Natural Disasters in Developing Countries. *Geomorphology* **2002**, *47*, 2–4. [CrossRef]
2. Collier, C.G. Flash flood forecasting: What are the limits of predictability? *Q. J. R. Meteorol. Soc. A J. Atmos. Sci. Appl. Meteorol. Phys. Oceanogr.* **2007**, *133*, 3–23. [CrossRef]
3. Angillieri, M.Y.E. Morphometric characterization of the Carrizal basin applied to the evaluation of flash floods hazard, San Juan, Argentina. *Quat. Int.* **2012**, *253*, 74–79. [CrossRef]
4. Drobnjak, S.; Milonjić, Z.; Dordević, D.; Simić, M. Flash flood susceptibility mapping using LiDAR-Derived DEM and machine learning algorithms: Ljubovida case study, Serbia. *Open Geosci.* **2025**, *17*, 20250859. [CrossRef]
5. Bashir, B. Morphometric Parameters and Geospatial Analysis for Flash Flood Susceptibility Assessment: A Case Study of Jeddah City along the Red Sea Coast, Saudi Arabia. *Water* **2023**, *15*, 870. [CrossRef]
6. Arabameri, A.; Saha, S.; Chen, W.; Roy, J.; Pradhan, B.; Bui, D.T. Flash flood susceptibility modelling using functional tree and hybrid ensemble techniques. *J. Hydrol.* **2020**, *587*, 125007. [CrossRef]
7. Fowler, H.J.; Lenderink, G.; Prein, A.F.; Westra, S.; Allan, R.P.; Ban, N.; Barbero, R.; Berg, P.; Blenkinsop, S.; Do, H.X.; et al. Anthropogenic intensification of short-duration rainfall extremes. *Nat. Rev. Earth Environ.* **2021**, *2*, 107–122. [CrossRef]
8. Wasko, C.; Nathan, R.; Stein, L.; O'Shea, D. Evidence of shorter more extreme rainfalls and increased flood variability under climate change. *J. Hydrol.* **2021**, *603*, 126994. [CrossRef]
9. Khalifa, A.; Bashir, B.; Alsalman, A.; Naik, S.P.; Nappi, R. Remotely Sensed Data, Morpho-Metric Analysis, and Integrated Method Approach for Flood Risk Assessment: Case Study of Wadi Al-Arish Landscape, Sinai, Egypt. *Water* **2023**, *15*, 1797. [CrossRef]
10. Ullah, A.; Farooq, R.; Ghumman, A.R.; Tanveer, M.E.; Tariq, M.A.U.R. Flash flood susceptibility assessment using an integrated geomorphologic framework in data-scarce arid and semi-arid regions. *Model. Earth Syst. Environ.* **2026**, *12*, 142. [CrossRef]
11. Nabinejad, S.; Schüttrumpf, H. Flood Risk Management in Arid and Semi-Arid Areas: A Comprehensive Review of Challenges, Needs, and Opportunities. *Water* **2023**, *15*, 3113. [CrossRef]
12. Dutal, H. Using morphometric analysis for assessment of flash flood susceptibility in the Mediterranean region of Turkey. *Environ. Monit. Assess.* **2023**, *195*, 582. [CrossRef] [PubMed]
13. Dano, U.L. Assessing the Impact of Anthropogenic Factors on Flash Floods in a Coastal City of Saudi Arabia. *Civ. Eng. Archit.* **2025**, *13*, 612–624. [CrossRef]
14. Stewart, I. Sustainable geoscience. *Nat. Geosci.* **2016**, *9*, 262. [CrossRef]
15. Alhamid, A.A.; Alfayzi, S.A.; Hamadto, M.A. A Sustainable Water Resources Management Plan for Wadi Hanifa in Saudi Arabia. *J. King Saud Univ.-Eng. Sci.* **2007**, *19*, 209–221. [CrossRef]

16. Dano, U.L.; Aboukorin, A.A.; Alshihri, F.S.; Alnaim, A.; Almutlaq, F.; Jamil, R.; Alqahtany, A.M.; Alshammari, M.S.; Almazroua, S.; Elhadi Abdalla, E.M. Assessment of Flood Hazard and Infrastructure Vulnerability Under Sea-Level Rise in Eastern Saudi Arabia: Implications of UN SDGs for Sustainable Cities. *Sustainability* **2026**, *18*, 2510. [CrossRef]
17. Abdelkareem, M. Targeting flash flood potential areas using remotely sensed data and GIS techniques. *Nat. Hazards* **2017**, *85*, 19–37. [CrossRef]
18. Carpenter, T.M.; Sperfslage, J.A.; Georgakakos, K.P.; Sweeney, T.; Fread, D.L. National threshold runoff estimation utilizing GIS in support of operational flash flood warning systems. *J. Hydrol.* **1999**, *224*, 21–44. [CrossRef]
19. Mahmood, S.; Ullah, S. Assessment of 2010 flash flood causes and associated damages in Dir Valley, Khyber Pakhtunkhwa Pakistan. *Int. J. Disaster Risk Reduct.* **2016**, *16*, 215–223. [CrossRef]
20. Alarifi, S.S.; Abdelkareem, M.; Abdalla, F.; Alotaibi, M. Flash Flood Hazard Mapping Using Remote Sensing and GIS Techniques in Southwestern Saudi Arabia. *Sustainability* **2022**, *14*, 4145. [CrossRef]
21. Manzoor, Z.; Ehsan, M.; Khan, M.B.; Manzoor, A.; Akhter, M.M.; Sohail, M.T.; Hussain, A.; Shafi, A.; Abu-Alam, T.; Abioui, M. Floods and flood management and its socio-economic impact on Pakistan: A review of the empirical literature. *Front. Environ. Sci.* **2022**, *10*, 1021862. [CrossRef]
22. Riveros, A.; Gunaratne, C.; Martinelli, M.; Weiland, F.C.S. A single framework for assessing flash flood and landslide susceptibility: An application to the Mediterranean Liguria region, Italy. *Nat. Hazards Earth Syst. Sci.* **2026**, *26*, 2437–2459. [CrossRef]
23. Adnan, M.S.G.; Dewan, A.; Zannat, K.E.; Abdullah, A.Y.M. The use of watershed geomorphic data in flash flood susceptibility zoning: A case study of the Karnaphuli and Sangu river basins of Bangladesh. *Nat. Hazards* **2019**, *99*, 425–448. [CrossRef]
24. Sharif, H.O.; Al-Juaidi, F.H.; Al-Othman, A.; Al-Dousary, I.; Fadda, E.; Jamal-Uddeen, S.; Elhassan, A. Flood hazards in an urbanizing watershed in Riyadh, Saudi Arabia. *Geomat. Nat. Hazards Risk* **2016**, *7*, 702–720. [CrossRef]
25. Al-Ahmadi, K.; Al-Ahmadi, S. Spatiotemporal variations in rainfall-topographic relationships in southwestern Saudi Arabia. *Arab. J. Geosci.* **2014**, *7*, 3309–3324. [CrossRef]
26. Elsebaie, I.H.; Kawara, A.Q. Modeling groundwater recharge potential zones in the Wadi Yalamlam, Saudi Arabia. *Front. Water* **2024**, *6*, 1387741. [CrossRef]
27. Dawod, G.M.; Mirza, M.N.; Al-Ghamdi, K.A. GIS-Based Spatial Mapping of Flash Flood Hazard in Makkah City, Saudi Arabia. *J. Geogr. Inf. Syst.* **2011**, *03*, 225–231. [CrossRef]
28. Elsebaie, I.H.; Kawara, A.Q.; Alnahit, A.O. Mapping and Assessment of Flood Risk in the Wadi Al-Lith Basin, Saudi Arabia. *Water* **2023**, *15*, 902. [CrossRef]
29. Elkhrachy, I. Flash Flood Hazard Mapping Using Satellite Images and GIS Tools: A case study of Najran City, Kingdom of Saudi Arabia (KSA). *Egypt. J. Remote Sens. Space Sci.* **2015**, *18*, 261–278. [CrossRef]
30. Schmidt, D.L.; Hadley, D.G.; Stoeser, D.B. Late Proterozoic crustal history of the Arabian Shield, southern Najd Province, Kingdom of Saudi Arabia. In *Evolution and Mineralization of the Arabian–Nubian Shield*; Publication authorized by the Director, U.S. Geological Survey; Arabian Ministry of Petroleum & Mineral Resources: Riyadh, Saudi Arabia, 1979; Volume 2, pp. 41–58. [CrossRef]
31. Elawadi, E.; Mogren, S.; Ibrahim, E.; Batayneh, A.; Al-Bassam, A. Utilizing potential field data to support delineation of groundwater aquifers in the southern Red Sea coast, Saudi Arabia. *J. Geophys. Eng.* **2012**, *9*, 327–335. [CrossRef]
32. Johnson, P.R.; Kattanl, F.H.; Wooden, J.L. Implications of SHRIMP and Microstructural Data on the Age and Kinematics of Shearing in the Asir Terrane, Southern Arabian Shield, Saudi Arabia. *Gondwana Res.* **2001**, *4*, 172–173. [CrossRef]
33. Patton, P.C.; Baker, V.R. Morphometry and floods in small drainage basins subject to diverse hydrogeomorphic controls. *Water Resour. Res.* **1976**, *12*, 941–952. [CrossRef]
34. Khalifa, A.; Bashir, B.; Alsalman, A.; Bachir, H. Morphometric-Hydro Characterization of the Coastal Line between El-Qussier and Marsa-Alam, Egypt: Preliminary Flood Risk Signatures. *Appl. Sci.* **2022**, *12*, 6264. [CrossRef]
35. Mesa, L.M. Morphometric analysis of a subtropical Andean basin (Tucumán, Argentina). *Environ. Geol.* **2006**, *50*, 1235–1242. [CrossRef]
36. Bharadwaj, A.K.; Thirumalaivasan, D.; Shankar, C.P.; Madhavan, N. Morphometric Analysis of Adyar Watershed. Available online: https://www.iosrjournals.org/iosr-jmce/papers/NCCAMABS/Volume-2/25.pdf (accessed on 1 June 2026).
37. Horton, R.E. Erosional development of streams and their drainage basins; Hydrophysical approach to quantitative morphology. *Bull. Geol. Soc. Am.* **1945**, *56*, 275–370. [CrossRef]
38. Strahler, A.N. Quantitative geomorphology of drainage basins is channel networks. In *Applied Hydrology*; Vent, T.C., Ed.; McGraw Hill Book Company: New York, NY, USA, 1964; pp. 39–79.
39. Singh, P.; Gupta, A.; Singh, M. Hydrological inferences from watershed analysis for water resource management using remote sensing and GIS techniques. *Egypt. J. Remote Sens. Space Sci.* **2014**, *17*, 111–121. [CrossRef]
40. Şen, Z.; Khiyami, H.A.; Al-Harthy, S.G.; Al-Ammawi, F.A.; Al-Balkhi, A.B.; Al-Zahrani, M.I. Flash flood inundation map preparation for wadis in arid regions. *Arab. J. Geosci.* **2013**, *6*, 3563–3572. [CrossRef]

41. El Shamy, I. Recent recharge and flash flooding opportunities in the Eastern Desert, Egypt. *Ann. Geol. Surv. Egypt* **1992**, *18*, 323–334.
42. El-Shamy, I.Z. Quantitative geomorphometry and surface runoff control in Wadi Qena, Central Eastern Desert, Egypt. In Proceedings of the Geophysical Society of the 6th Annals, Cairo, Egypt, 22–23 March 1988; pp. 13–26.
43. Nasir, M.J.; Iqbal, J.; Ahmad, W. Flash flood risk modeling of swat river sub-watershed: A comparative analysis of morphometric ranking approach and El-Shamy approach. *Arab. J. Geosci.* **2020**, *13*, 1082. [CrossRef]
44. Horton, R.E. The Rôle of infiltration in the hydrologic cycle. *Eos Trans. Am. Geophys. Union* **1933**, *14*, 446–460. [CrossRef]
45. Pilgrim, D.H.; Chapman, T.G.; Doran, D.G. Problèmes de la mise au point de modèles pluie-écoulement dans les régions arides et semi-arides. *Hydrol. Sci. J.* **1988**, *33*, 379–400. [CrossRef]
46. Ouerghi, S.; Al-Mannai, A.A.M. The approach of automatic drainage anomalies extraction for active tectonic detection: Jizan coastal plain (Southwestern of Saudi Arabia). *Geocarto Int.* **2026**, *41*, 2600181. [CrossRef]
47. Abdelfattah, A.K.; Abdelrahman, K.; Qaysi, S.; Fnais, M.; Al-amri, A. Earthquake recurrence characteristics for potential seismic zones in the southern Red Sea region and their hazard implications on Jizan city. *J. King Saud Univ. Sci.* **2022**, *34*, 101880. [CrossRef]
48. Abu-Abdullah, M.M.; Youssef, A.M.; Maerz, N.H.; Abu-Alfadail, E.; Al-Harbi, H.M.; Al-Saadi, N.S. A flood riskmanagement programofwadi bayshdam on the downstream area: An integration of hydrologic and hydraulicmodels, Jizan region, KSA. *Sustainability* **2020**, *12*, 1069. [CrossRef]
49. Masoud, M.H.Z.; Basahi, J.M.; Zaidi, F.K. Assessment of artificial groundwater recharge potential through estimation of permeability values from infiltration and aquifer tests in unconsolidated alluvial formations in coastal areas. *Environ. Monit. Assess.* **2019**, *191*, 31. [CrossRef] [PubMed]
50. Radwan, F.; Alazba, A.; Mossad, A. Watershed morphometric analysis of Wadi Baish Dam catchment area using integrated GIS-based approach. *Arab. J. Geosci.* **2017**, *10*, 256. [CrossRef]
51. AlAli, A.M.; Salih, A.; Hassaballa, A. Geospatial-Based Analytical Hierarchy Process (AHP) and Weighted Product Model (WPM) Techniques for Mapping and Assessing Flood Susceptibility in the Wadi Hanifah Drainage Basin, Riyadh Region, Saudi Arabia. *Water* **2023**, *15*, 1943. [CrossRef]
52. Soni, S. Assessment of morphometric characteristics of Chakrar watershed in Madhya Pradesh India using geospatial technique. *Appl. Water Sci.* **2017**, *7*, 2089–2102. [CrossRef]
53. Shekar, P.R.; Mathew, A. Morphometric analysis of watersheds: A comprehensive review of data sources, quality, and geospatial techniques. *Watershed Ecol. Environ.* **2024**, *6*, 13–25. [CrossRef]
54. Kabite, G.; Gessesse, B. Hydro-geomorphological characterization of Dhidhessa River Basin, Ethiopia. *Int. Soil Water Conserv. Res.* **2018**, *6*, 175–183. [CrossRef]
55. Nourani, V.; Zanardo, S. Wavelet-based regularization of the extracted topographic index from high-resolution topography for hydro-geomorphic applications. *Hydrol. Process.* **2014**, *28*, 1345–1357. [CrossRef]
56. Saha, S.; Das, J.; Mandal, T. Investigation of the watershed hydro-morphologic characteristics through the morphometric analysis: A study on Rayeng basin in Darjeeling Himalaya. *Environ. Chall.* **2022**, *7*, 100463. [CrossRef]
57. Khan, M.Y.A.; ElKashouty, M. Watershed prioritization and hydro-morphometric analysis for the potential development of Tabuk Basin, Saudi Arabia using multivariate statistical analysis and coupled RS-GIS approach. *Ecol. Indic.* **2023**, *154*, 110766. [CrossRef]
58. Moore, I.D.; Grayson, R.B.; Ladson, A.R. Digital terrain modelling: A review of hydrological, geomorphological, and biological applications. *Hydrol. Process.* **1991**, *5*, 3–30. [CrossRef]
59. Khalifa, A. Application of Remote sensing techniques in discrimination of rock units and preliminary assessment of tectonic activity using ASTER and ALOSE-PALSAR data at Gabal Delihimmi, Central Eastern Desert, Egypt. *Egypt. J. Geol.* **2023**, *67*, 287–298. [CrossRef]
60. Wei, Y.; Gan, S.; Yuan, X.; Hu, L.; Gao, S. Analysis of Topographic Feature Parameters of Dinosaur Valley Ring Tectonic Geomorphology Based on the Advanced Land Observing Satellite Digital Elevation Model (ALOS DEM). *Appl. Sci.* **2023**, *13*, 3137. [CrossRef]
61. Yang, J.; Zhao, J.; Hao, P.; Zhang, A.; Li, X.; Tu, R.; Zhang, Z. Evaluating the Impact of Multi-Source Digital Elevation Model Quality on Archeological Predictive Modeling: An Integrated Framework Based on Machine Learning and SHAP-Based Interpretability Analysis. *Remote Sens.* **2026**, *18*, 961. [CrossRef]
62. Khalifa, A.; Bashir, B.; Alsalman, A.; Öğretmen, N. Morpho-tectonic assessment of the abu-dabbab area, eastern desert, egypt: Insights from remote sensing and geospatial analysis. *ISPRS Int. J. Geoinf.* **2021**, *10*, 784. [CrossRef]
63. Khal, M.; Algouti, A.; Algouti, A.; Akdim, N.; Stankevich, S.A.; Menenti, M. Evaluation of open Digital Elevation Models: Estimation of topographic indices relevant to erosion risk in the Wadi M'Goun watershed, Morocco. *AIMS Geosci.* **2020**, *6*, 231–257. [CrossRef]
64. Roy, S.K.; Chowdhury, M.A. Morphometric analysis and watershed delineation of the Karnaphuli river basin: A comparative study using different DEMs in Chittagong, Bangladesh. *River* **2024**, *3*, 426–437. [CrossRef]

65. Mohd Iqbal, H.S. Watershed Prioritization using Morphometric and Land Use/Land Cover Parameters of Dudhganga Catchment Kashmir Valley India using Spatial Technology. *J. Geophys. Remote Sens.* **2014**, *3*, 1000115. [CrossRef]
66. Haokip, P.; Khan, M.A.; Choudhari, P.; Kulimushi, L.C.; Qaraev, I. Identification of erosion-prone areas using morphometric parameters, land use land cover and multi-criteria decision-making method: Geo-informatics approach. *Environ. Dev. Sustain.* **2022**, *24*, 527–557. [CrossRef]
67. Schumm, S.A. Evolution of drainage systems and slopes in badlands at Perth Amboy, New Jersey. *Bull. Geol. Soc. Am.* **1956**, *67*, 597–646. [CrossRef]
68. Dzwairo, R.; Singh, S.K.; Patel, A. Soil erosion susceptibility assessment through morphometric analysis and morphotectonic implications in Rietspruit sub-basin, South Africa. *Environ. Dev. Sustain.* **2024**, *27*, 16503–16524. [CrossRef]
69. Wilford, D.J.; Sakals, M.E.; Innes, J.L.; Sidle, R.C.; Bergerud, W.A. Recognition of debris flow, debris flood and flood hazard through watershed morphometrics. *Landslides* **2004**, *1*, 61–66. [CrossRef]
70. Spyrou, E.; Maroukian, H.; Evelpidou, N. Application of morphotectonic indices for assessing active tectonics: A case study of Acheron river basin. *J. Struct. Geol.* **2024**, *187*, 105240. [CrossRef]
71. Chorley, R.; Horton, R.E. 1945: Erosional development of streams and their drainage basins: Hydrophysical approach to quantitative morphology. Bulletin of the Geological Society of America 56, 2 75-370. *Prog. Phys. Geogr.* **1995**, *19*, 533–554. [CrossRef]
72. Alam, A.; Ahmed, B.; Sammonds, P. Flash flood susceptibility assessment using the parameters of drainage basin morphometry in SE Bangladesh. *Quat. Int.* **2021**, *575–576*, 295–307. [CrossRef]
73. Waikar, M.L.; Nilawar, A.P. Morphometric Analysis of a Drainage Basin Using Geographical Information System: A Case study. *Int. J. Multidiscip. Curr. Res.* **2014**, *2*, 179–184.
74. Das, B.C.; Islam, A.; Sarkar, B. Drainage Basin Shape Indices to Understanding Channel Hydraulics. *Water Resour. Manag.* **2022**, *36*, 2523–2547. [CrossRef]
75. Maou, A.; Souadnia, S.; Faqeih, K.; AlAmri, A.; Hadji, R.; Alamri, S.; Harizi, K.; Alamery, E.; Sonia, G.; Leila, B.; et al. Assessing flash flood occurrences and hazard zones along the mediterranean coasts: A GIS and mapping techniques approach in the Wadi Saf Saf Basin, Northeast Algeria. *Front. Earth Sci.* **2025**, *13*, 1594364. [CrossRef]
76. Chopra, R.; Dhiman, R.D.; Sharma, P.K. Morphometric analysis of sub-watersheds in Gurdaspur district, Punjab using remote sensing and GIS techniques. *J. Indian Soc. Remote Sens.* **2005**, *33*, 531–539. [CrossRef]
77. Khalifa, A.; Çakir, Z.; Owen, L.A.; Kaya, Ş. Morphotectonic analysis of the East Anatolian Fault, Turkey. *Turk. J. Earth Sci.* **2018**, *27*, 110–126. [CrossRef]
78. Tukura, N.G.; Akalu, M.M.; Hussein, M.; Befekadu, A. Morphometric analysis and sub-watershed prioritization of Welmal watershed, Ganale-Dawa River Basin, Ethiopia: Implications for sediment erosion. *J. Sediment. Environ.* **2021**, *6*, 121–130. [CrossRef]
79. Samal, D.R.; Gedam, S.S.; Nagarajan, R. GIS based drainage morphometry and its influence on hydrology in parts of Western Ghats region, Maharashtra, India. *Geocarto Int.* **2015**, *30*, 755–778. [CrossRef]
80. Mansour, M.M.; Nasr, M.; Fujii, M.; Yoshimura, C.; Ibrahim, M.G. 4 th International Conference on Hydroscience & Engineering Identification of A Practical Method and A Set of Morphometric Parameters for Flash Flood Potential Prioritization. Available online: https://earthexplorer.usgs.gov/ (accessed on 1 June 2026).
81. Bashir, B.; Alsalman, A. Geospatial Analysis for Tectonic Assessment and Soil Erosion Prioritization: A Case Study of Wadi Al-Lith, Red Sea Coast, Saudi Arabia. *Appl. Sci.* **2023**, *13*, 2523. [CrossRef]
82. El Osta, M.; El Sabri, M.; Masoud, M. Environmental sensitivity of flash flood hazard based on surface water model and GIS techniques in Wadi El Azariq, Sinai, Egypt. *Environ. Technol. Innov.* **2021**, *22*, 101522. [CrossRef]
83. Bajabaa, S.; Masoud, M.; Al-Amri, N. Flash flood hazard mapping based on quantitative hydrology, geomorphology and GIS techniques (case study of Wadi Al Lith, Saudi Arabia). *Arab. J. Geosci.* **2014**, *7*, 2469–2481. [CrossRef]
84. Cyr, A.J.; Granger, D.E.; Olivetti, V.; Molin, P. Quantifying rock uplift rates using channel steepness and cosmogenic nuclide-determined erosion rates: Examples from northern and southern Italy. *Lithosphere* **2010**, *2*, 188–198. [CrossRef]
85. Costache, R. Flash-flood Potential Index mapping using weights of evidence, decision Trees models and their novel hybrid integration. *Stoch. Environ. Res. Risk Assess.* **2019**, *33*, 1375–1402. [CrossRef]
86. Greenwood, W.R.; Stoeser, D.B.; Fleck, R.J.; Stacey, J.S. *Late Proterozoic Island-Arc Complexes and Tectonic Belts in the Southern Part of the Arabian Shield, Kingdom of Saudi Arabia*; U.S. Geological Survey, USGS Publications Warehouse: Jiddah, Saudi Arabia, 1982. [CrossRef]
87. Khan, M.Y.A.; ElKashouty, M.; Subyani, A.M.; Tian, F. Morphometric Determination and Digital Geological Mapping by RS and GIS Techniques in Aseer–Jazan Contact, Southwest Saudi Arabia. *Water* **2023**, *15*, 2438. [CrossRef]
88. Abdelaal, O.H.; Abdehafeez, T.H.; Taha, A.I. Evaluation of Renewable Water Resources and Estimating of Aquifer Parameters in Wadi Hubuna, Southwestern Part of Saudi Arabia. *Iraqi Geol. J.* **2023**, *56*, 19–37. [CrossRef]

89. Sumi, T.; Kantoush, S.A.; Saber, M. Natural Disaster Science and Mitigation Engineering: DPRI Reports Wadi Flash Floods Challenges and Advanced Approaches for Disaster Risk Reduction. Available online: http://www.springer.com/series/11773 (accessed on 1 June 2026).
90. Ghanim, A.A.J.; Al-Areeq, A.M.; Benaafi, M.; Al-Suwaiyan, M.S.; Aghbari, A.A.A.; Alyami, M. Mapping Groundwater Potential Zones in the Habawnah Basin of Southern Saudi Arabia: An AHP- and GIS-based Approach. *Sustainability* **2023**, *15*, 75. [CrossRef]
91. Subyani, A.M. Topographic and Seasonal Influences on Precipitation Variability in Southwest Saudi Arabia. *J. King Abdulaziz Univ.-Earth Sci.* **2000**, *11*, 89–102. [CrossRef]
92. Ghrefat, H.; Hakami, A.; Ibrahim, E.; Mogren, S.; Qaysi, S.; Abdelrahman, K.; Zaidi, F.K. Damage Assessment of a Salt Dome in Jizan, Southwestern Saudi Arabia, Using High Spatial Resolution Remote Sensing Data. *Front. Earth Sci.* **2021**, *9*, 700337. [CrossRef]
93. Alhumimidi, M.S. Geotechnical assessment of near-surface sediments and their hazardous impact: Case study of Jizan city, southwestern Saudi Arabia. *J. King Saud Univ. Sci.* **2020**, *32*, 2195–2201. [CrossRef]
94. Mogren, S. Saltwater Intrusion in Jizan Coastal Zone, Southwest Saudi Arabia, Inferred from Geoelectric Resistivity Survey. *Int. J. Geosci.* **2015**, *6*, 286–297. [CrossRef]
95. Basahi, J.M.; Masoud, M.H.; Zaidi, S.F. Saudi Arabia Identifying of Flash Flood-Prone Areas Based upon the Physical Characteristics of Semi-Arid Basins (Case Study of Wadi Baysh Basin, Southwest Saudi Arabia). In Proceedings of the 8 International Conference on Water Resources and Arid Environments (ICWRAE 8), Riyadh, Saudi Arabi, 22–24 January 2019; pp. 109–120.
96. Ahmad, W.; Nasir, M.J.; Iqbal, J. Flash flood susceptibility modeling for drainage basins of Dir Lower Khyber-Pakhtunkhwa: A comparative analysis of morphometric ranking and El-Shamy's approach. In *Proceedings of the Remote Sensing for Agriculture, Ecosystems, and Hydrology XXII*; Neale, C.M., Maltese, A., Eds.; SPIE: Washington, DC, USA, 2020; p. 11. [CrossRef]
97. Islam, M.N.; Zamreeq, A.O.; Ismail, M.; Habeebullah, T.M.A.; Ghulam, A.S. Jazan Rainfall's Seasonal Shift in Saudi Arabia: Evidence of a Changing Regional Climate. *Atmosphere* **2025**, *16*, 300. [CrossRef]
98. Youssef, A.M.; Abu-Abdullah, M.M.; Alfadail, E.A.; Skilodimou, H.D.; Bathrellos, G.D. The devastating flood in the arid region a consequence of rainfall and dam failure: Case study, al-lith flood on 23th November 2018, Kingdom of Saudi Arabia. *Z. Fur Geomorphol.* **2021**, *63*, 115–136. [CrossRef]


**Disclaimer/Publisher's Note:** The statements, opinions and data contained in all publications are solely those of the individual author(s) and contributor(s) and not of MDPI and/or the editor(s). MDPI and/or the editor(s) disclaim responsibility for any injury to people or property resulting from any ideas, methods, instructions or products referred to in the content.